Journal of Asian Earth Sciences 130 (2016) 223–238

Contents lists available at ScienceDirect

Journal of Asian Earth Sciences

journal homepage: www.elsevier.com/locate/jseaes

Full length Article

# Zircon U-Pb age and geochemical constraints on the origin and tectonic implication of Cadomian (Ediacaran-Early Cambrian) magmatism in SE Turkey

Melahat Beyarslan [a,*], Yu-Chin Lın [b], A. Feyzi Bingöl [a], Sun-Lin Chung [b,c]

[a] Department of Geological Engineering, Firat University, Elazığ, Turkey
[b] Department of Geosciences, National Taiwan University, Taipei, Taiwan
[c] Institute of Earth Sciences, Academia Sinica, Taipei, Taiwan

ARTICLE INFO

*Article history:*
Received 25 February 2016
Received in revised form 4 August 2016
Accepted 9 August 2016
Available online 10 August 2016

*Keywords:*
Cadomian
Gneisses
Zircon U-Pb and Hf isotopes
Pütürge
SE Anatolia

ABSTRACT

The Bitlis-Pütürge Massifs and Derik volcanics that crop out in the Southeast Anatolian Belt are parts of the Cadomian domain in Anatolia where relicts of the oldest continental crust of Turkey are exposed. The Bitlis-Pütürge Massifs contain a Neoproterozoic basement, with overlying Phanerozoic rocks that were imbricated, metamorphosed and thrust over the edge of Arabia during the Alpine orogeny. The basement consists mainly of granitic to tonalitic augen gneisses and metagranites, associated with schists, amphibolites and paragneisses. Based on whole-rock geochemical data, the augen gneisses are interpreted to have protoliths crystallized from subduction zone magmas. This study conducted the first zircon dating on two augen gneisses that gave $^{206}Pb/^{238}U$ dates of 551 ± 6 and 544 ± 4 Ma, interpreted as the formation ages of the Pütürge Massif, broadly coeval to those of the Bitlis metagranites and the Derik volcanics that occurred from ca. 581 to 529 Ma (the Ediacaran-early Cambrian). The εHf(t) values (+1.2 to −5.3) of the dated zircons, with crustal model ages ($T^c_{DM}$) from 1.4 to 1.8 Ga, indicate that formation of the Pütürge Massif involves an older, most likely the Mesoproterozoic, continental crust component. Similar to the Bitlis-Pütürge gneisses, coeval basement rocks are widespread in the Tauride-Anatolide platform (e.g., the Menderes Massif). All these dispersed Cadomian basement rocks are interpreted as fragments of the Ediacaran-Early Cambrian continental arcs bordering the active margin of northern Gondwana.


## 1. Introduction

Turkey is located in the middle of the Alpine–Himalayan orogenic belt, which resulted from the closure of different branches of the Tethyan Ocean, along with the amalgamation of two major continents, Gondwana in south and Laurasia in north. Many Late Neoproterozoic to Early Paleozoic (600–500 Ma) blocks within the Alpine–Himalayan orogenic belt (Fig. 1a) were generated by the Ediacaran-Cambrian arc-type magmatism or so-called the Cadomian events, as suggested by paleomagnetic data, distribution of fossils, detrital zircon geochronology and zircon U-Pb age data of magmatic rocks and gneisses (e.g., Nance and Murphy, 1996; Fernandez-Suarez et al., 2000, 2002; Stampfli, 2000; Nance et al., 2002, 2008; Neubauer, 2002; Keppie et al., 2003; Murphy et al., 2004; Winchester et al., 2006; Linnemann et al., 2007; Ustaömer et al., 2009, 2012; Cocks and Torsvik, 2011; Gürsu et al., 2015; von Raumer et al., 2015; Avigad et al., 2016). The Neoproterozoic-Cambrian time frame was dominated by the growth of the Gondwana Supercontinent that resulted from a long-lived orogenic construction, starting from the breakup of Rodinia (~870–800 Ma) to the final amalgamation of rifted blocks in Cambrian times (e.g. Dalziel, 1991; Meert, 2003; Boger and Miller, 2004; Collins and Pisarevsky, 2005; Cawood, 2005; Cawood and Buchan, 2007; Li et al., 2008; Torsvik and Cocks, 2013; Nance et al., 2014). The terminal assembly that occurred – older than or about 600 Ma was achieved through complex accretion of various continental blocks involving a prolonged collisional assembly between East and West Gondwana (Meert, 2003; Collins and Pisarevsky, 2005; Meert and Lieberman, 2008) and development of subduction systems along the margins of the Gondwana supercontinent, e.g., the Terra Australis Orogen and the North India Orogen (Boger and Miller, 2004; Cawood, 2005; Murphy et al., 2011).

In this paper, we report the first zircon U-Pb ages of augen gneisses from the Pütürge Massif, an important albeit less studied component of the Southeast Anatolian Belt as part of the Cadomian domain in Turkey. We then combine regional literature with our field, geochemical, geochronological data obtained from the

* Corresponding author.
*E-mail address:* melahat.beyarslan@gmail.com (M. Beyarslan).

http://dx.doi.org/10.1016/j.jseaes.2016.08.006
1367-9120/

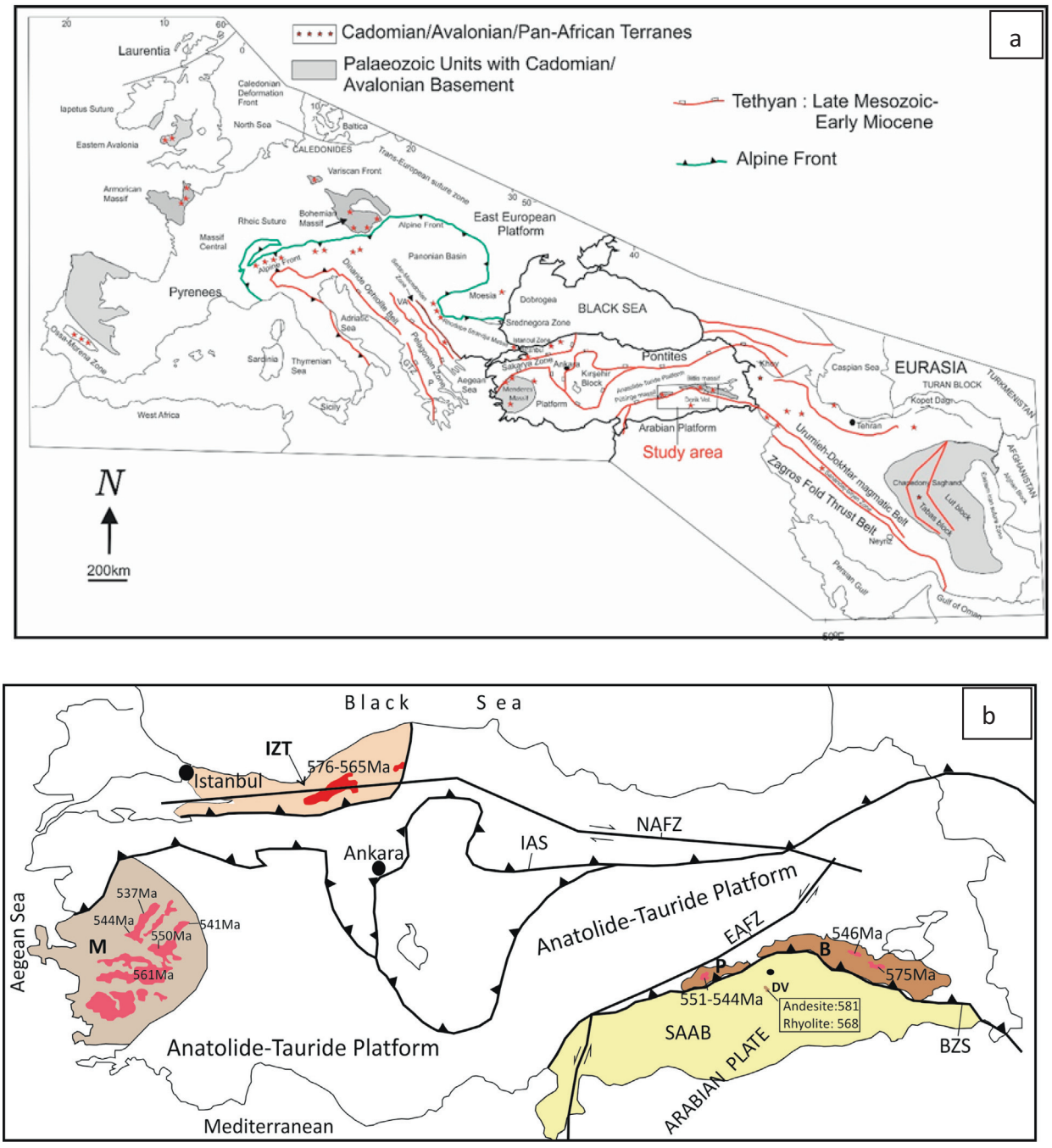


**Fig. 1.** (a) Tectonic map showing the locations of Cadomian–Avalonian basement units in Europe and the Eastern Mediterranean area. Data sources: Ustaömer et al. (2005, 2009, 2012), Yılmaz-Şahin et al. (2014) and Moghadam et al. (2015). (b) Distribution of Cadomian Terrenes in Turkey. IZT: Istanbul-Zonguldak Terrane, M: Menderes Massif, P: Pütürge Massif, B: Bitlis Massif, SAAB: South Anatolian Autochthone Belt (SAAB), IAS: Izmir-Ankara Suture, BZS: Bitlis-Zagros Suture, EAFZ: East Anatolian Fault Zone, NAFZ: North Anatolian Fault Zone. Adapted from Ustaömer et al. (2012), Gürsu et al. (2015) and Okay and Nikishin (2015).

Bitlis-Pütürge metamorphic Massifs and associated Derik volcanics in the Arabian Plate to interpret the Ediacaran-Terreneuvian tectonic evolution of the South Anatolian Belt in Turkey, with further implications for the Cadomian events related to the formation and subsequent breakup of the Gondwana Supercontinent.

## 2. Geological background

### 2.1. Bitlis-Pütürge Massifs

The Late Neoproterozoic-Cambrian basement rocks of Turkey are generally interpreted as the dispersed fragments of the Cadomian active margin (Ustaömer et al., 2009, 2012; Gürsu et al., 2015). Recent efforts to understand the Cadomian basement in Turkey emphasize dating of metamorphosed magmatics (granites and gabbros) and gneissic rocks and provenance analysis of Paleozoic sedimentary units (e.g., Ustaömer et al., 2009, 2012; Zlatkin et al., 2013; Yılmaz-Şahin et al., 2014; Gürsu et al., 2015; Candan et al., 2015; Avigad et al., 2016). Gondwana-derived Late Proterozoic/Early Paleozoic units in Turkey mainly crop out in five separate Alpine tectonic units; (i) the Istanbul-Zonguldak Terrane (IZT), (ii) the Tauride-Anatolide Platform (TAP), (iii) Menderes Massif, (iv) Bitlis-Pütürge Massifs and (v) the South Anatolian Autochthone Belt (Fig. 1b).

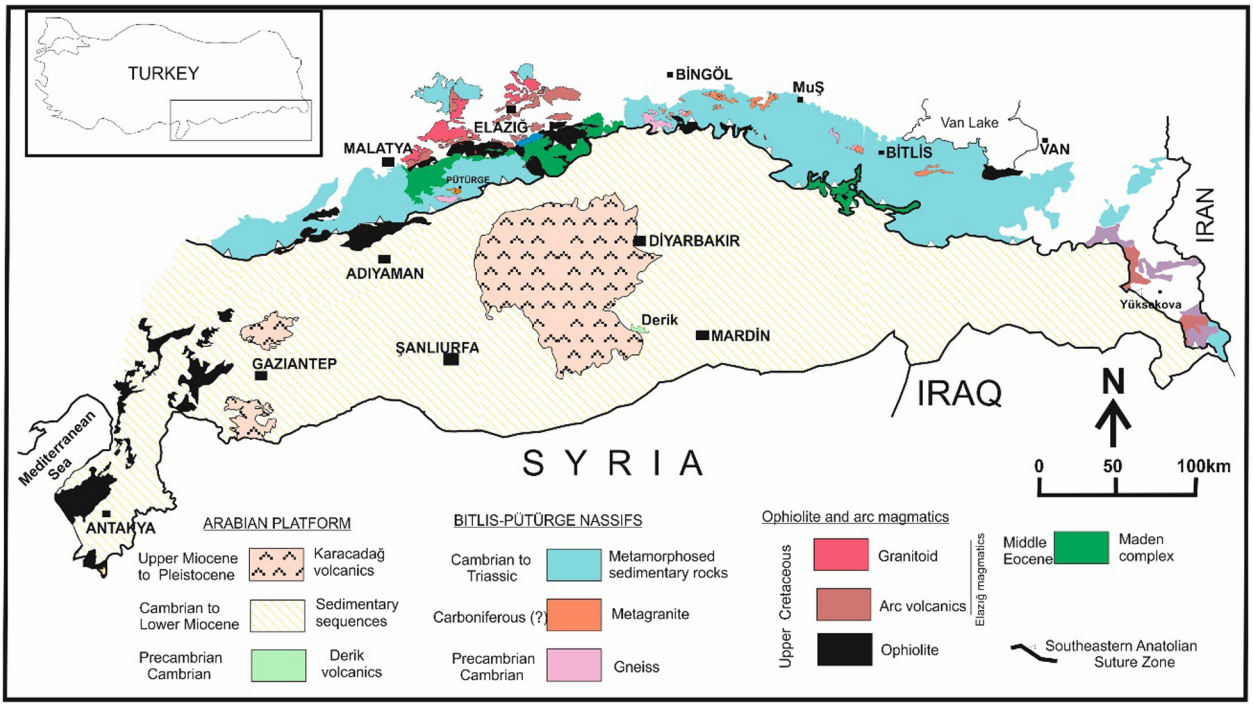


**Fig. 2.** Simplified geological map of the Bitlis and Pütürge Massifs (modified from 1/500,000-scale geological map) (MTA, 2004).

The Bitlis-Pütürge metamorphic Massif represents one of the metamorphic Massifs of southeast Anatolia (Fig. 2); including the Malatya, Keban, Engizek, and Binboga Massifs. The Bitlis and Pütürge Massifs are regional-scale allochthonous units that show similar stratigraphic successions. They may be interpreted as parts of a once-united giant tectono-stratigraphic unit that has been disrupted and fragmented during orogeny (Yılmaz and Yiğitbaş, 1991). They comprise a high grade metamorphic lower unit and a lower grade metamorphic cover as the upper unit forming an envelope around the lower unit (Göncüoğlu and Turhan, 1984; Erdem, 1994; Erdem and Bingöl, 1995) (Fig. 3A and B).

The high grade metamorphic lower units of the two Massifs are similar and are composed of granitoid gneiss (augen gneiss) ranging in composition from quartz diorite, tonalite to granodiorite, various schists, amphibolites, and meta-granites. The augen gneisses are the lowermost unit of the Bitlis-Pütürge Massifs (Göncüoğlu and Turhan, 1984; Erdem, 1994; Erdem and Bingöl, 1995). The augens consist of K-feldspar reaching up to 10–15 cm long (Fig. 4a).

There are some eclogite relicts in the central part at Mt. Gablor (Okay et al., 1985) and in the Kesandere valley in the easternmost of the Bitlis Massif (Oberhänsli et al., 2014) in the high grade lower unit rocks. The Kesandere eclogites formed during the middle Late Cretaceous, whereas a Pan-African age was assumed for the Mt. Gabor eclogites (Okay et al., 1985; Oberhänsli et al., 2014). The Mt. Gablor eclogitic bodies were produced by eclogitic metamorphism of the subducted plate during the Ediacaran-early Cambrian southward subduction and exhumed into the high-grade metamorphic units at the final stage of subduction, whereas the Kesander eclogites were formed by metamorphism of the subducted plate during the Late Cretaceous northward subduction and exhumed into the other units at the final stage of subduction (Oberhänsli et al., 2012, 2014). The schists, composed of biotite, muscovite, garnet and amphibole, are crosscut by amphibolites (Fig. 4b) and metagranites. The meta-granites cut the augen gneisses, amphibolites and schists, but they do not cut the Permian formations, thus, they should have formed before Permian time (Erdem and Bingöl, 1995). According to Göncüoğlu and Turhan (1984), the metagranites are unaffected by the predominant regional metamorphism. Regardless of variable age data, Göncüoğlu and Turhan (1984) suggested a Middle Devonian–Late Permian crystallization age for the metagranitic rocks based mainly on the reported field evidence that some of the granites cut Devonian meta-sedimentary formations but never cut the Mesozoic cover (Fig. 3A and B).

The lower unit rocks underwent high grade metamorphism related possibly to the final amalgamation of exotic terranes with northeastern Gondwana or to the development of a subsequent subduction zone along the Gondwana margin (Collins and Pisarevsky, 2005). The lower unit is overlain by muscovite schist that contain mid-Devonian fossils with kyanite bearing quartzite lenses, garnet staurolite micaschist and Permian recrystallized limestones. There are some andesitic and dacitic dykes belonging to the Middle Eocene Maden Complex within the Permian recrystallized limestones (Yıldırım, 2010). In this respect, as well as in the degree of metamorphism of the lower unit, the Bitlis-Pütürge Massifs resemble the Menderes Massif. The Triassic unit of Bitlis Massif, which is missing in Pütürge Massif consists of recrystallized limestones and calc-schists grading upward into metashales, metatuffs, metadiabases and metabasalts and finally metaconglomerates, metamudstones and shales (Oberhänsli et al., 2012). The Pütürge metamorphics depositionally overlain by the Middle Eocene Maden Complex whereas the Bitlis Massif overlain by the Middle Miocene to Quaternary volcanics in the North. All these rocks are exposed by thrusts onto the neo-autochthonous Arabian Platform and Neo-Tethyan ophiolites along its southern contacts (Perinçek, 1980; Perinçek and Özkaya, 1981; Yazgan, 1983, 1984; Michard et al., 1984; Aktaş and Robertson, 1984; Yazgan and Chessex, 1991; Yılmaz, 1993; Yılmaz et al., 1993; Yiğitbaş and Yılmaz, 1996; Yılmaz and Yıldırım, 1996). The lower unit rocks and upper unit were metamorphosed under greenschistfacies conditions during Upper Cretaceous (Yazgan and Chessex, 1991; Erdem and Bingöl, 1995).

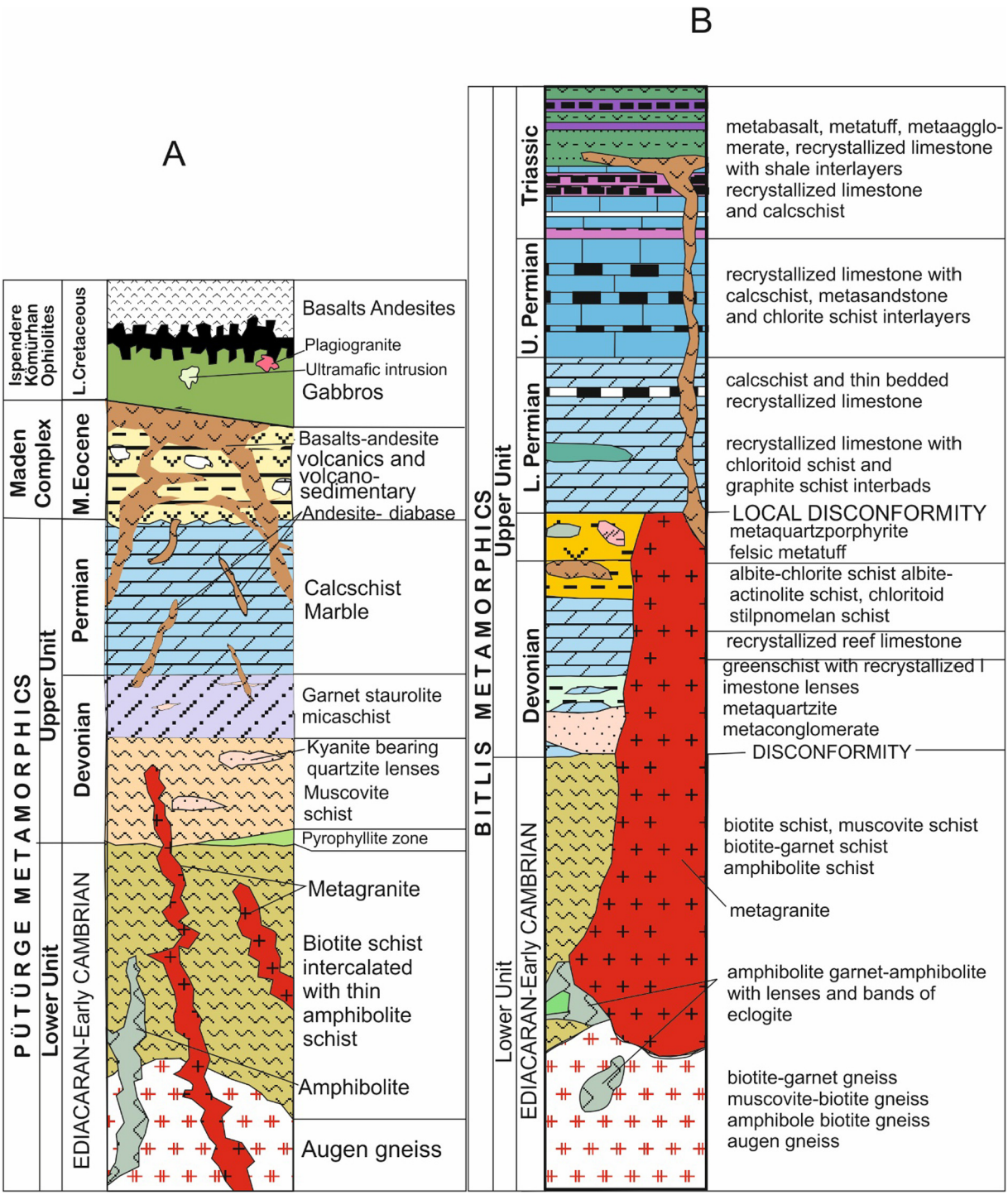


**Fig. 3.** (A) Lithologic column of the Pütürge Massif adapted from Erdem and Bingöl (1995). (B) Lithologic column of the Bitlis Massif adapted from Göncüoglu and Turhan (1984).

### 2.2. Derik area

Derik area (Mardin) is located along the northernmost margin of the Arabian Plate. The basal section of the Derik area consists of non-metamorphosed volcanic rocks, conglomerates and fine/coarse sandstones. This succession is known as the "Infracambrian of SE Anatolia" (Ketin, 1966). The basal detrital was reported first by Kellogg (1960). "Derik volcanics" composed of non-metamorphic succession of basaltic lavas and subordinate volcanoclastics, however the base of it is not exposed (Göncüoglu and Kozlu, 2000). Overlying deposits include, in ascending order, conglomerates, a limestone horizon, and a redbed type succession. The lack of biostratigraphic data and rapid lateral variations characterize the first depositional sequence, which is coeval with the ultimate Pan-African/Cadomian post-collisional events that affected northern Gondwana (Ghienne et al., 2010). The volcanic rocks are divided into three sub-units by Gürsu et al. (2015). (a) A thick sub-unit composed of early stage andesitic lavas and rhyolite with rare siltstone/sandstone intercalations. Rhyolites associated with pyroclastic rocks are observed within early-stage


**Fig. 4.** Field photos of old basement rocks in the Pütürge massif. (a) Augen gneiss, (b) micaschists intruded by amphibolite dyke.

andesitic rocks, (b) late stage andesitic rocks and (c) pyroclastic rocks (agglomerates/volcanic breccias).

## 3. Petrography

### 3.1. Augen gneisses

The augen gneisses from Pütürge Massif are coarse- to very coarse-grained rocks composed of microcline + quartz + red brown biotite + muscovite ± zircon ± apatite ± ilmenite mineral assemblage. The augen gneisses also contain chlorite ± green biotite ± albite ± epidote mineral assemblage. This second mineral assemblage should belong to the retrograde phase that effect the lower and upper units during Late Cretaceous.

The K-feldspar augens mostly consist of single crystals of K-feldspar. The augens are pink to milky white, and can reach up to 10–15 cm long in the fine- to medium-grained granoblastic and lepidoblastictextures. Lepidoblastic matrix composed of fine to coarse-grained quartz, plagioclase and K-feldspar and medium- to coarse-grained biotite, with rare small muscovite plates. Inclusions of quartz, muscovite, zircon, and minor biotite are common. The lepidoblastic texture may be separated from augen of granoblastic textures or in direct contact with them.-The augen gneisses from Bitlis are plagioclase-augen gneisses (Göncüoğlu and Turhan, 1984). They are coarse grained rocks composed of quartz, oligoclase, biotite, garnet, muscovite. The augen consists of single crystals of plagioclase. All metagranites have a well-preserved igneous mineralogy but they show granoblastic and lepidoblastic and mylonitic textures. The metagranites mainly consist of plagioclase, K-feldspar, quartz and biotite, with minor muscovite ± amphibole ± muscovite ± zircon ± titanite ± garnet ± opaque minerals. The proportion of these minerals has shown changes in different lithologies. In the

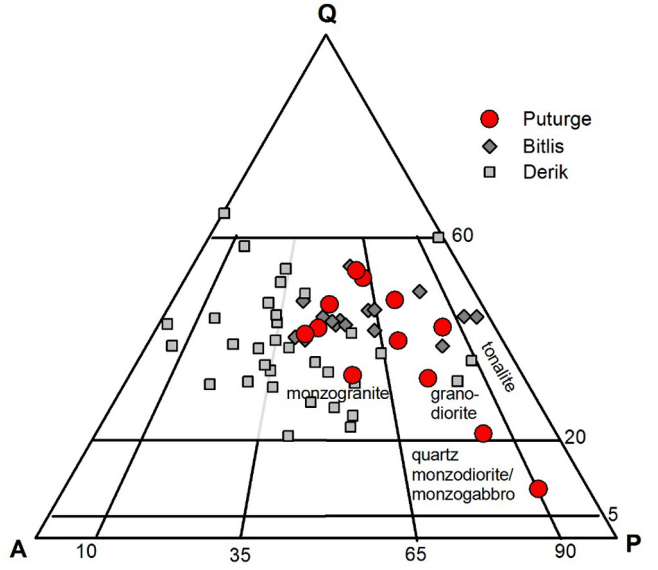


**Fig. 5.** QAP nomenclature diagram with normative mineral composition for augen gneisses of Pütürge massif (red circles, this study), metamorphics of Bitlis massif (gray diamonds, Ustaömer et al., 2012), and Derik volcanics (gray squares, Gürsu et al., 2015). (For interpretation of the references to color in this figure legend, the reader is referred to the web version of this article.)

QAP (Quartz-Alkali feldspar-Plagioclase) ternary diagram (Fig. 5; Streckeisen, 1976), the augen gneisses and metagranites plot in the tonalite to monzo-granite fields.

### 3.2. Derik volcanics (Gürsu et al., 2015)

Based on their mineralogical composition and textural characteristics, the Derik Volcanics in the Derik (Mardin) area can be divided into three lithological units, namely andesite, rhyolite and mafic dykes. Andesites are porphyritic, with abundant phenocrysts set in an originally partly glassy, now devitrified fine groundmass consisting mainly of microcrystalline plagioclase and opaque minerals. The phenocrysts are mainly characterized by plagioclase, amphibole and minor pyroxene and biotite.

The rhyolites display porphyritic texture. Phenocryst mineral phases include quartz, sanidine, sodic plagioclase, with occasional hornblende, while zircon, apatite, titanite and pyrite are accessory minerals. Plagioclase phenocrysts are lath- or tabular-shaped, euhedral to subhedral, ranging up to 1 cm in size and show zoning and albite-type polysynthetic twinning. Alkali feldspar phenocrysts are rare in most samples. Quartz is commonly subhedral, with straight edges. This quartz also occurs in the matrix, filling the interstitial spaces. The groundmass is fine-grained anhedral granular and is composed of quartz, alkali feldspar and plagioclase with intergranular opaques, chlorite and accessory apatite and zircon.

## 4. Analytical methods

Twelve representative samples of metamorphic rocks from the Pütürge Massif have been analyzed for their major and trace element composition (Table 1). Four of these samples were analyzed (13TK-51 to -54) at the Shen-su Sun Memorial Lab of Department of Geosciences, National Taiwan University, where major elements were measured by X-ray fluorescence (XRF) techniques on fused glass beads using a Rigaku® RIX-2000 spectrometer and trace elements were measured by the inductively coupled plasma-mass spectrometry (ICP-MS) using an Agilent 7500cs equipment. The detailed analytical procedures were the same as those reported

**Table 1**
Major and trace elements for augen gneiss samples from Pütürge massif.

| | 13TK51 | 13TK52 | 13TK53 | 13TK54 | P132 | P136 | P144 | P145 | P152 | P154 | P161 | P168 |
|---|---|---|---|---|---|---|---|---|---|---|---|---|
| $SiO_2$ | 71.3 | 60.1 | 63.5 | 67.9 | 57.3 | 70.6 | 71.6 | 67.8 | 67.5 | 69.8 | 70.8 | 69.9 |
| $TiO_2$ | 0.51 | 0.87 | 1.19 | 0.63 | 1.46 | 0.57 | 0.62 | 0.61 | 0.53 | 1.42 | 0.52 | 0.49 |
| $Al_2O_3$ | 14.2 | 18.1 | 19.5 | 14.7 | 16.7 | 15.7 | 13.5 | 13.8 | 14.4 | 14.6 | 14.3 | 13.5 |
| $Fe_2O_3$ | 2.36 | 8.97 | 1.62 | 4.39 | 6.09 | 2.42 | 2.78 | 4.88 | 3.27 | 2.59 | 2.81 | 2.41 |
| MnO | 0.02 | 0.13 | 0.03 | 0.04 | 0.08 | 0.02 | 0.02 | 0.02 | 0.02 | 0.02 | 0.02 | 0.05 |
| MgO | 0.94 | 3.41 | 1.14 | 1.37 | 3.16 | 1.21 | 0.98 | 1.45 | 1.69 | 1.37 | 0.98 | 1.83 |
| CaO | 1.68 | 1.47 | 2.27 | 1.31 | 6.09 | 0.87 | 1.81 | 1.29 | 1.43 | 1.62 | 1.20 | 2.47 |
| $Na_2O$ | 4.75 | 1.53 | 7.42 | 3.27 | 4.45 | 5.28 | 4.35 | 3.34 | 3.18 | 3.13 | 4.67 | 3.19 |
| $K_2O$ | 2.59 | 3.05 | 1.32 | 4.29 | 1.59 | 1.27 | 2.04 | 4.11 | 4.47 | 2.41 | 2.61 | 2.41 |
| $P_2O_5$ | 0.14 | 0.21 | 0.03 | 0.14 | 0.35 | 0.13 | 0.15 | 0.14 | 0.12 | 0.13 | 0.13 | 0.14 |
| LOI | | | | | 2.51 | 1.14 | 2.07 | 1.84 | 1.98 | 1.47 | 1.27 | 2.53 |
| Total | 98.5 | 97.8 | 98.0 | 98.0 | 99.8 | 99.2 | 99.9 | 99.3 | 98.6 | 98.6 | 99.3 | 98.9 |
| Sc | 19 | 22 | 10 | 19 | 26 | 10 | 12 | 19 | 14 | 11 | 12 | 17 |
| V | 39 | 138 | 88 | 56 | 179 | 54 | 118 | 98 | 59 | 58 | 49 | 96 |
| Cr | 82 | 111 | 102 | 47 | 292 | 79 | 102 | 131 | 128 | 97 | 87 | 59 |
| Mn | 181 | 956 | 197 | 282 | 657 | 183 | 179 | 182 | 167 | 195 | 176 | 162 |
| Co | 5.1 | 19 | 3.9 | 7.4 | 5.8 | 5.2 | 4.6 | 6.5 | 6.1 | 4.6 | 7.4 | 8.9 |
| Ni | 44 | 59 | 55 | 22 | 15 | 43 | 68 | 52 | 54 | 48 | 42 | 39 |
| Cu | 5.2 | 40 | 6.6 | 7.9 | 11 | 18 | 17 | 27 | 29 | 34 | 12 | 11 |
| Zn | 22 | 205 | 0 | 29 | 42 | 12 | 42 | 17 | 21 | 22 | 46 | 19 |
| Ga | 21 | 23 | 22 | 19 | 19 | 22 | 21 | 19 | 21 | 20 | 21 | 19 |
| Rb | 76 | 128 | 50 | 134 | 62 | 75 | 126 | 112 | 114 | 66 | 63 | 76 |
| Sr | 105 | 162 | 208 | 124 | 250 | 131 | 159 | 151 | 149 | 157 | 208 | 164 |
| Y | 34 | 40 | 28 | 34 | 45 | 35 | 32 | 39 | 41 | 38 | 35 | 34 |
| Zr | 264 | 168 | 238 | 259 | 310 | 213 | 187 | 227 | 201 | 235 | 219 | 149 |
| Nb | 15 | 12 | 17 | 13 | 26 | 14 | 12 | 12 | 15 | 13 | 16 | 17 |
| Cs | 0.60 | 8.0 | 0.54 | 1.8 | 6.0 | 2.9 | 1.9 | 0.97 | 6.9 | 0.8 | 0.9 | 6.3 |
| Ba | 366 | 606 | 163 | 875 | 350 | 147 | 443 | 287 | 854 | 521 | 381 | 201 |
| La | 39 | 35 | 20 | 42 | 28 | 38 | 27 | 24 | 60 | 45 | 46 | 27 |
| Ce | 79 | 70 | 69 | 86 | 66 | 76 | 71 | 53 | 69 | 81 | 85 | 70 |
| Pr | 9.2 | 8.4 | 8.7 | 10 | 9.2 | 8.9 | 9.1 | 8.8 | 9.1 | 8.7 | 9.1 | 8.9 |
| Nd | 33 | 34 | 33 | 37 | 33 | 32 | 34 | 26 | 33 | 36 | 38 | 34 |
| Sm | 6.6 | 6.3 | 5.2 | 6.6 | 6.4 | 6.2 | 5.8 | 6.4 | 5.7 | 6.6 | 6.3 | 6.1 |
| Eu | 0.96 | 1.4 | 0.88 | 1.2 | 0.96 | 1.1 | 0.91 | 1.2 | 0.97 | 0.91 | 1.2 | 0.98 |
| Gd | 6.0 | 6.6 | 5.0 | 6.6 | 6.0 | 6.4 | 6.5 | 6.1 | 6.3 | 6.4 | 6.5 | 6.2 |
| Tb | 0.96 | 1.1 | 0.78 | 1.0 | 0.98 | 1.1 | 0.83 | 1.0 | 0.81 | 0.92 | 0.94 | 1.1 |
| Dy | 5.7 | 6.3 | 4.4 | 5.7 | 5.4 | 5.8 | 6.2 | 6.1 | 6.0 | 5.8 | 5.4 | 5.2 |
| Ho | 1.2 | 1.3 | 0.90 | 1.1 | 1.2 | 1.2 | 1.1 | 1.2 | 1.2 | 1.1 | 1.1 | 0.96 |
| Er | 3.3 | 3.7 | 2.7 | 3.1 | 3.3 | 3.3 | 3.0 | 3.1 | 3.2 | 3.4 | 3.1 | 2.9 |
| Tm | 0.49 | 0.55 | 0.40 | 0.45 | 0.46 | 0.51 | 0.48 | 0.47 | 0.44 | 0.48 | 0.43 | 0.52 |
| Yb | 3.2 | 3.5 | 2.6 | 2.7 | 3.2 | 3.2 | 3.4 | 3.3 | 2.8 | 2.8 | 3.1 | 3.2 |
| Lu | 0.45 | 0.53 | 0.40 | 0.40 | 0.43 | 0.48 | 0.52 | 0.42 | 0.41 | 0.44 | 0.41 | 0.53 |
| Hf | 6.5 | 4.3 | 6.2 | 6.9 | 6.2 | 5.3 | 6.7 | 6.2 | 6.4 | 6.3 | 5.7 | 6.4 |
| Ta | 1.3 | 0.86 | 1.0 | 0.94 | 1.1 | 1.0 | 1.1 | 1.1 | 1.0 | 0.96 | 1.1 | 1.1 |
| Pb | 1.2 | 24 | 1.1 | 5.8 | 4.2 | 1.2 | 1.4 | 1.2 | 3.4 | 2.4 | 1.3 | 2.2 |
| Th | 19 | 10 | 5.0 | 21 | 15 | 17 | 13 | 14 | 21 | 20 | 18 | 8.0 |
| U | 2.5 | 2.9 | 3.1 | 2.6 | 2.9 | 2.8 | 2.9 | 2.8 | 2.7 | 3.1 | 3.0 | 2.7 |

in Lin et al. (2012). The other eight samples (P132-P168) were analyzed at the ACME Analytical Laboratories, Vancouver, Canada, using ICP emission spectrography for major elements and some trace elements (Ba, Nb, Ni, Sr, Sc, Y and Zr), and ICP-MS for other trace elements including rare earth elements.

Two augen gneiss samples, 13TK51 and 13TK54, were subjected to *in situ* zircon U–Pb dating and Lu-Hf isotope analysis (Tables 2 and 3). Euhedral to subhedral zircons with few cracks and inclusions were picked out under binocular with hands, and then mounted on the epoxy resin and polished for cathodoluminescence (CL) imaging that was taken for observing the internal structure of each zircon grain and selecting suitable position for isotope analysis. Zircons were first dated by using the laser ablation ICP-MS facilities at Department of Geosciences, National Taiwan University. The detailed analytical methods with analytical precision can be found in Chiu et al. (2009) and Shao et al. (2015).

Zircon Lu-Hf isotopes were measured using a Neptune multi-collector ICP-MS equipped with a Lambda Physik COMpex UV-193 laser-ablation system at the Institute of Geology and Geophysics, Chinese Academy of Sciences in Beijing, China. Detailed analytical procedures are described by Wu et al. (2006). Lu-Hf isotopic calculations are made with following equations:

$\lambda_{Lu\text{-}Hf} = 1.86 \times 10^{-11}$ y (Scherer et al., 2001)

$\varepsilon Hf(T) = [(^{176}Hf/^{177}Hf)^{T}_{Sample}/(^{176}Hf/^{177}Hf)^{T}_{CHUR} - 1] \times 10^4$ (Patchett and Tastumoto, 1981)

$(^{176}Hf/^{177}Hf)^{T}_{Sample} = (^{176}Hf/^{177}Hf)^{0}_{Sample} - (^{176}Lu/^{177}Hf)^{0}_{Sample} \times (e^{\lambda T} - 1)$; $(^{176}Hf/^{177}Hf)^{T}_{CHUR} = (^{176}Hf/^{177}Hf)^{0}_{CHUR} - (^{176}Lu/^{177}Hf)^{0}_{CHUR} \times (e^{\lambda T} - 1)$

$(^{176}Hf/^{177}Hf)^{0}_{CHUR} = 0.282772$; $(^{176}Lu/^{177}Hf)^{0}_{CHUR} = 0.0332$ (Blichert-Toft and Albarède, 1997)

$(^{176}Hf/^{177}Hf)_{DM} = 0.28325$; $(^{176}Lu/^{177}Hf)_{DM} = 0.0384$ (Nowell et al., 1998; Griffin et al., 2000)

$(^{176}Lu/^{177}Hf)_{mean\ crust} = 0.015$ (Griffin et al., 2000)

$f_{CC} = (0.015/0.0332) - 1 = -0.5482$; $f_{DM} = (0.0384/0.0332) - 1 = 0.1566$

**Table 2**
Zircon U–Pb LA-ICP-MS data of the Pütürge augen gneisses.

| Spot | U (ppm) | Th/U | U-Th-Pb ratios | | | | | | | | Ages (Ma) | | | | | | | |
|---|---|---|---|---|---|---|---|---|---|---|---|---|---|---|---|---|---|---|
| | | | $^{207}Pb/^{235}U$ | 1σ | $^{206}Pb/^{238}U$ | 1σ | $^{207}Pb/^{206}Pb$ | 1σ | $^{208}Pb/^{232}Th$ | 1σ | $^{206}Pb/^{238}U$ | 1σ | $^{207}Pb/^{206}Pb$ | 1σ | $^{207}Pb/^{235}U$ | 1σ | Inferred age | 1σ |
| *13TK51 (wt. mean age = 551 ± 6 (2σ), n = 21)* | | | | | | | | | | | | | | | | | | |
| 13TK51-01 | 546 | 0.10 | 0.72306 | 0.01039 | 0.08727 | 0.00107 | 0.06010 | 0.00038 | 0.02367 | 0.00079 | 539 | 6 | 607 | 13 | 552 | 6 | 539 | 6 |
| 13TK51-02 | 375 | 0.21 | 0.72249 | 0.01075 | 0.08553 | 0.00106 | 0.06127 | 0.0004 | 0.02582 | 0.00086 | 529 | 6 | 649 | 14 | 552 | 6 | 529 | 6 |
| 13TK51-04 | 432 | 0.11 | 0.72370 | 0.01077 | 0.08759 | 0.00108 | 0.05993 | 0.00039 | 0.02466 | 0.00089 | 541 | 6 | 601 | 14 | 553 | 6 | 541 | 6 |
| 13TK51-05 | 638 | 0.30 | 0.73391 | 0.01063 | 0.08775 | 0.00108 | 0.06066 | 0.00039 | 0.02547 | 0.00089 | 542 | 6 | 627 | 13 | 559 | 6 | 542 | 6 |
| 13TK51-06 | 553 | 0.50 | 0.71782 | 0.01064 | 0.08586 | 0.00106 | 0.06065 | 0.00040 | 0.02623 | 0.00094 | 531 | 6 | 627 | 14 | 549 | 6 | 531 | 6 |
| 13TK51-07 | 497 | 0.19 | 0.72812 | 0.01089 | 0.08839 | 0.00109 | 0.05976 | 0.00040 | 0.02467 | 0.00093 | 546 | 6 | 595 | 14 | 555 | 6 | 546 | 6 |
| 13TK51-09 | 196 | 0.52 | 0.79191 | 0.01458 | 0.09288 | 0.00120 | 0.06184 | 0.00055 | 0.02525 | 0.00103 | 573 | 7 | 669 | 18 | 592 | 8 | 573 | 7 |
| 13TK51-10 | 333 | 0.32 | 0.73255 | 0.01151 | 0.08808 | 0.00110 | 0.06033 | 0.00043 | 0.02552 | 0.00105 | 544 | 7 | 615 | 15 | 558 | 7 | 544 | 7 |
| 13TK51-12 | 366 | 0.37 | 0.72512 | 0.01146 | 0.08713 | 0.00109 | 0.06037 | 0.00043 | 0.02540 | 0.00110 | 539 | 6 | 617 | 15 | 554 | 7 | 539 | 6 |
| 13TK51-13 | 265 | 0.24 | 0.74731 | 0.01177 | 0.09074 | 0.00113 | 0.05973 | 0.00042 | 0.03091 | 0.00119 | 560 | 7 | 594 | 14 | 567 | 7 | 560 | 7 |
| 13TK51-14 | 399 | 0.12 | 0.75781 | 0.01139 | 0.09095 | 0.00113 | 0.06043 | 0.00040 | 0.02823 | 0.00114 | 561 | 7 | 619 | 13 | 573 | 7 | 561 | 7 |
| 13TK51-15 | 714 | 0.19 | 0.73914 | 0.01074 | 0.09154 | 0.00113 | 0.05857 | 0.00037 | 0.02824 | 0.00115 | 565 | 7 | 551 | 13 | 562 | 6 | 565 | 7 |
| 13TK51-16 | 477 | 0.10 | 0.74282 | 0.01122 | 0.09142 | 0.00113 | 0.05894 | 0.00039 | 0.0267 | 0.00116 | 564 | 7 | 565 | 13 | 564 | 7 | 564 | 7 |
| 13TK51-17 | 729 | 0.08 | 0.73337 | 0.01088 | 0.08973 | 0.00111 | 0.05928 | 0.00039 | 0.02911 | 0.0013 | 554 | 7 | 577 | 13 | 559 | 6 | 554 | 7 |
| 13TK51-18 | 486 | 0.54 | 0.73423 | 0.01126 | 0.09045 | 0.00113 | 0.05888 | 0.00040 | 0.02865 | 0.00129 | 558 | 7 | 563 | 14 | 559 | 7 | 558 | 7 |
| 13TK51-19 | 565 | 0.87 | 0.74946 | 0.01146 | 0.09185 | 0.00114 | 0.05919 | 0.00040 | 0.02905 | 0.00136 | 566 | 7 | 574 | 14 | 568 | 7 | 566 | 7 |
| 13TK51-20 | 512 | 0.09 | 0.74657 | 0.01099 | 0.09088 | 0.00112 | 0.05958 | 0.00039 | 0.03038 | 0.00121 | 561 | 7 | 588 | 13 | 566 | 6 | 561 | 7 |
| 13TK51-21 | 530 | 0.09 | 0.74381 | 0.01452 | 0.09127 | 0.00112 | 0.05911 | 0.00064 | 0.02823 | 0.00034 | 563 | 7 | 571 | 22 | 565 | 8 | 563 | 7 |
| 13TK51-22 | 544 | 0.11 | 0.73312 | 0.01163 | 0.08962 | 0.00112 | 0.05933 | 0.00042 | 0.03168 | 0.00134 | 553 | 7 | 579 | 14 | 558 | 7 | 553 | 7 |
| 13TK51-23 | 385 | 0.11 | 0.7655 | 0.01275 | 0.08946 | 0.00113 | 0.06206 | 0.00047 | 0.02574 | 0.00116 | 552 | 7 | 676 | 15 | 577 | 7 | 552 | 7 |
| 13TK51-24 | 880 | 0.09 | 0.7449 | 0.01081 | 0.0910 | 0.00112 | 0.05937 | 0.00038 | 0.02975 | 0.00127 | 561 | 7 | 581 | 13 | 565 | 6 | 561 | 7 |
| *13TK54 (wt. mean age = 544 ± 4 (2σ), n = 21)* | | | | | | | | | | | | | | | | | | |
| 13TK54-01 | 361 | 0.3 | 0.69330 | 0.01079 | 0.08797 | 0.00114 | 0.05716 | 0.00039 | 0.02731 | 0.00095 | 544 | 7 | 498 | 15 | 535 | 6 | 544 | 7 |
| 13TK54-02 | 420 | 0.13 | 0.70548 | 0.01078 | 0.08983 | 0.00116 | 0.05696 | 0.00038 | 0.02658 | 0.00098 | 555 | 7 | 490 | 14 | 542 | 6 | 555 | 7 |
| 13TK54-03R | 517 | 0.17 | 0.68929 | 0.01040 | 0.08759 | 0.00113 | 0.05708 | 0.00038 | 0.02694 | 0.00101 | 541 | 7 | 495 | 14 | 532 | 6 | 541 | 7 |
| 13TK54-05 | 544 | 0.15 | 0.70665 | 0.01057 | 0.08905 | 0.00114 | 0.05756 | 0.00038 | 0.02859 | 0.00112 | 550 | 7 | 513 | 14 | 543 | 6 | 550 | 7 |
| 13TK54-07 | 470 | 0.1 | 0.68154 | 0.01053 | 0.08874 | 0.00115 | 0.05571 | 0.00038 | 0.02704 | 0.00118 | 548 | 7 | 441 | 15 | 528 | 6 | 548 | 7 |
| 13TK54-08 | 342 | 0.57 | 0.75986 | 0.01189 | 0.08893 | 0.00115 | 0.06197 | 0.00043 | 0.02968 | 0.00124 | 549 | 7 | 673 | 14 | 574 | 7 | 549 | 7 |
| 13TK54-09 | 516 | 0.11 | 0.70183 | 0.01072 | 0.08953 | 0.00115 | 0.05686 | 0.00038 | 0.03672 | 0.00166 | 553 | 7 | 486 | 14 | 540 | 6 | 553 | 7 |
| 13TK54-11 | 596 | 0.13 | 0.71176 | 0.01090 | 0.09000 | 0.00116 | 0.05736 | 0.00039 | 0.02883 | 0.00140 | 556 | 7 | 505 | 14 | 546 | 6 | 556 | 7 |
| 14TK54-15 | 439 | 0.12 | 0.72719 | 0.01215 | 0.08778 | 0.00106 | 0.06009 | 0.00047 | 0.02599 | 0.00134 | 542 | 6 | 607 | 16 | 555 | 7 | 542 | 6 |
| 14TK54-16 | 305 | 0.25 | 0.70183 | 0.01089 | 0.08577 | 0.00107 | 0.05935 | 0.00041 | 0.02735 | 0.00102 | 530 | 6 | 580 | 15 | 540 | 6 | 530 | 6 |
| 13TK54-18 | 248 | 0.48 | 0.71745 | 0.01160 | 0.08879 | 0.00111 | 0.05861 | 0.00043 | 0.02888 | 0.00118 | 548 | 7 | 553 | 15 | 549 | 7 | 548 | 7 |
| 13TK54-19 | 363 | 0.10 | 0.69419 | 0.01075 | 0.08703 | 0.00108 | 0.05785 | 0.00040 | 0.02561 | 0.00109 | 538 | 6 | 524 | 15 | 535 | 6 | 538 | 6 |
| 13TK54-20 | 286 | 0.54 | 0.70747 | 0.01145 | 0.08804 | 0.0011 | 0.05828 | 0.00043 | 0.03114 | 0.00136 | 544 | 7 | 540 | 16 | 543 | 7 | 544 | 7 |
| 13TK54-21 | 483 | 0.14 | 0.71534 | 0.01764 | 0.08631 | 0.00106 | 0.06011 | 0.00104 | 0.02665 | 0.00032 | 534 | 6 | 608 | 36 | 548 | 10 | 534 | 6 |
| 13TK54-22 | 560 | 0.42 | 0.71181 | 0.01092 | 0.08875 | 0.0011 | 0.05818 | 0.00040 | 0.02808 | 0.00126 | 548 | 7 | 537 | 14 | 546 | 6 | 548 | 7 |
| 13TK54-24 | 310 | 0.19 | 0.73432 | 0.01197 | 0.08748 | 0.0011 | 0.06089 | 0.00045 | 0.02808 | 0.00136 | 541 | 7 | 635 | 15 | 559 | 7 | 541 | 7 |
| 13TK54-25 | 597 | 0.09 | 0.71654 | 0.01009 | 0.08896 | 0.00109 | 0.05842 | 0.00036 | 0.02994 | 0.00100 | 549 | 6 | 546 | 12 | 549 | 6 | 549 | 6 |
| 13TK54-26 | 563 | 0.13 | 0.76147 | 0.01655 | 0.08938 | 0.00111 | 0.06179 | 0.00079 | 0.02751 | 0.00033 | 552 | 7 | 667 | 25 | 575 | 10 | 552 | 7 |
| 13TK54-27 | 545 | 0.11 | 0.72998 | 0.01049 | 0.08799 | 0.00108 | 0.06017 | 0.00038 | 0.02923 | 0.00103 | 544 | 6 | 610 | 13 | 557 | 6 | 544 | 6 |
| 13TK54-28 | 457 | 0.15 | 0.69251 | 0.01019 | 0.08530 | 0.00105 | 0.05888 | 0.00038 | 0.02636 | 0.00095 | 528 | 6 | 563 | 13 | 534 | 6 | 528 | 6 |
| 13TK54-29 | 598 | 0.11 | 0.72824 | 0.01053 | 0.08782 | 0.00108 | 0.06014 | 0.00038 | 0.02855 | 0.00107 | 543 | 6 | 609 | 13 | 556 | 6 | 543 | 6 |

Note: Zircon U-Pb isotopes were measured using a Laser-ablation ICP-MS at the Department of Geosciences, National Taiwan University, Taipei, Taiwan. Detailed analytical procedures are described by Chiu et al. (2009).

**Table 3**
In situ zircon Lu-Hf isotopic data of the Pütürge augen gneisses.

| Spot | Age (Ma) | | U (ppm) | Th/U | $^{176}Yb/^{177}Hf$ | 2σ | $^{176}Lu/^{177}Hf$ | 2σ | $^{176}Hf/^{177}Hf$ | 2σ | $^{176}Hf/^{177}Hf$ i | $\varepsilon_{Hf}(T)$ | $T_{DM}$ (Ma) | $T^{C}_{DM}$ (Ma) |
|---|---|---|---|---|---|---|---|---|---|---|---|---|---|---|
| *13TK51* | | | | | | | | | | | | | | |
| 1 | 539 | 6 | 546 | 0.10 | 0.065 | 0.0008 | 0.0026 | 2.80E−05 | 0.282473 | 1.90E−05 | 0.2824 | 0.4 | 1151 | 1474 |
| 2 | 529 | 6 | 375 | 0.21 | 0.033 | 0.0001 | 0.0013 | 5.30E−06 | 0.282454 | 1.80E−05 | 0.2824 | −0.1 | 1139 | 1495 |
| 4 | 541 | 6 | 638 | 0.30 | 0.039 | 0.0002 | 0.0016 | 6.90E−06 | 0.282422 | 1.80E−05 | 0.2824 | −1.1 | 1194 | 1567 |
| 5 | 542 | 6 | 553 | 0.50 | 0.042 | 0.0004 | 0.0016 | 1.40E−05 | 0.282379 | 2.00E−05 | 0.2824 | −2.6 | 1255 | 1662 |
| 6 | 531 | 6 | 497 | 0.19 | 0.047 | 0.0011 | 0.0019 | 4.60E−05 | 0.282495 | 2.20E−05 | 0.2825 | 1.2 | 1096 | 1413 |
| 7 | 546 | 6 | 196 | 0.52 | 0.06 | 0.0002 | 0.0024 | 5.90E−06 | 0.282461 | 1.90E−05 | 0.2824 | 0.1 | 1163 | 1494 |
| 9 | 573 | 7 | 366 | 0.37 | 0.028 | 0.0001 | 0.0011 | 2.00E−06 | 0.282361 | 2.30E−05 | 0.2823 | −2.3 | 1261 | 1671 |
| 10 | 544 | 7 | 265 | 0.24 | 0.033 | 0.0005 | 0.0013 | 1.80E−05 | 0.282414 | 1.80E−05 | 0.2824 | −1.2 | 1195 | 1576 |
| 12 | 539 | 6 | 714 | 0.19 | 0.02 | 0.0002 | 0.0008 | 5.20E−06 | 0.282439 | 1.70E−05 | 0.2824 | −0.2 | 1144 | 1510 |
| 13 | 560 | 7 | 477 | 0.10 | 0.048 | 0.0003 | 0.0019 | 1.20E−05 | 0.282436 | 4.70E−05 | 0.2824 | −0.3 | 1182 | 1531 |
| 14 | 561 | 7 | 729 | 0.08 | 0.052 | 0.0002 | 0.002 | 7.30E−06 | 0.282437 | 1.80E−05 | 0.2824 | −0.3 | 1187 | 1532 |
| 15 | 565 | 7 | 486 | 0.54 | 0.06 | 0.0012 | 0.0024 | 4.20E−05 | 0.28231 | 2.50E−05 | 0.2823 | −4.8 | 1383 | 1822 |
| 16 | 564 | 7 | 565 | 0.87 | 0.05 | 0.0002 | 0.0019 | 1.00E−05 | 0.282408 | 1.70E−05 | 0.2824 | −1.2 | 1223 | 1590 |
| 17 | 554 | 7 | 512 | 0.09 | 0.075 | 0.0011 | 0.0029 | 3.90E−05 | 0.28233 | 3.20E−05 | 0.2823 | −4.5 | 1372 | 1794 |
| 18 | 558 | 7 | 530 | 0.09 | 0.061 | 0.0003 | 0.0023 | 6.50E−06 | 0.282439 | 2.30E−05 | 0.2824 | −0.4 | 1192 | 1535 |
| 19 | 566 | 7 | 544 | 0.11 | 0.051 | 0.0008 | 0.002 | 3.20E−05 | 0.282411 | 1.90E−05 | 0.2824 | −1.1 | 1223 | 1586 |
| 20 | 561 | 7 | 385 | 0.11 | 0.053 | 0.0003 | 0.0021 | 1.30E−05 | 0.282353 | 2.70E−05 | 0.2823 | −3.3 | 1309 | 1720 |
| 21 | 563 | 7 | 880 | 0.09 | 0.051 | 0.0005 | 0.002 | 2.00E−05 | 0.282399 | 1.90E−05 | 0.2824 | −1.6 | 1241 | 1615 |
| 22 | 553 | 7 | 546 | 0.10 | 0.058 | 0.0004 | 0.0023 | 1.20E−05 | 0.282463 | 2.20E−05 | 0.2824 | 0.4 | 1158 | 1484 |
| 23 | 552 | 7 | 375 | 0.21 | 0.051 | 0.0003 | 0.002 | 1.40E−05 | 0.282396 | 1.80E−05 | 0.2824 | −1.9 | 1245 | 1629 |
| 24 | 561 | 7 | 432 | 0.11 | 0.063 | 0.0007 | 0.0025 | 2.70E−05 | 0.282369 | 2.30E−05 | 0.2823 | −2.9 | 1301 | 1695 |
| *13TK54* | | | | | | | | | | | | | | |
| 1 | 544 | 7 | 361 | 0.30 | 0.024 | 0.0002 | 0.0009 | 7.50E−06 | 0.282444 | 2.50E−05 | 0.2824 | 0 | 1142 | 1500 |
| 2 | 555 | 7 | 420 | 0.13 | 0.04 | 0.0007 | 0.0016 | 2.30E−05 | 0.28243 | 2.00E−05 | 0.2824 | −0.4 | 1180 | 1539 |
| 3R | 541 | 7 | 544 | 0.15 | 0.045 | 0.0002 | 0.0018 | 9.00E−06 | 0.282391 | 2.80E−05 | 0.2824 | −2.2 | 1242 | 1639 |
| 5 | 550 | 7 | 470 | 0.10 | 0.051 | 0.0006 | 0.002 | 2.10E−05 | 0.282438 | 2.00E−05 | 0.2824 | −0.4 | 1184 | 1535 |
| 7 | 548 | 7 | 516 | 0.11 | 0.048 | 0.0002 | 0.0019 | 9.60E−06 | 0.28232 | 3.00E−05 | 0.2823 | −4.6 | 1349 | 1796 |
| 8 | 549 | 7 | 596 | 0.13 | 0.028 | 0.0005 | 0.0011 | 2.30E−05 | 0.282368 | 1.90E−05 | 0.2824 | −2.6 | 1253 | 1670 |
| 9 | 553 | 7 | 439 | 0.12 | 0.027 | 0.0003 | 0.0011 | 1.40E−05 | 0.282327 | 4.00E−05 | 0.2823 | −4 | 1310 | 1760 |
| 11 | 556 | 7 | 248 | 0.48 | 0.051 | 0.0006 | 0.0021 | 1.80E−05 | 0.282303 | 2.20E−05 | 0.2823 | −5.1 | 1378 | 1833 |
| 15 | 542 | 6 | 560 | 0.42 | 0.052 | 0.0005 | 0.002 | 1.80E−05 | 0.28236 | 1.70E−05 | 0.2823 | −3.4 | 1297 | 1715 |
| 16 | 530 | 6 | 310 | 0.19 | 0.022 | 0.0003 | 0.0009 | 1.10E−05 | 0.282416 | 1.90E−05 | 0.2824 | −1.3 | 1180 | 1571 |
| 18 | 548 | 7 | 563 | 0.13 | 0.032 | 0.0004 | 0.0012 | 1.50E−05 | 0.282312 | 3.10E−05 | 0.2823 | −4.7 | 1337 | 1800 |
| 19 | 538 | 6 | 545 | 0.11 | 0.036 | 0.0002 | 0.0015 | 7.60E−06 | 0.282416 | 2.20E−05 | 0.2824 | −1.3 | 1198 | 1579 |
| 20 | 544 | 7 | 457 | 0.15 | 0.026 | 0.0004 | 0.001 | 1.40E−05 | 0.2824 | 2.20E−05 | 0.2824 | −1.5 | 1204 | 1599 |
| 21 | 534 | 6 | 598 | 0.11 | 0.044 | 0.0002 | 0.0018 | 6.40E−06 | 0.282399 | 2.10E−05 | 0.2824 | −2 | 1230 | 1624 |
| 22 | 548 | 7 | 361 | 0.30 | 0.051 | 0.0004 | 0.002 | 1.30E−05 | 0.282348 | 2.70E−05 | 0.2823 | −3.7 | 1313 | 1737 |
| 24 | 541 | 7 | 517 | 0.17 | 0.045 | 0.0007 | 0.0018 | 2.60E−05 | 0.282303 | 3.00E−05 | 0.2823 | −5.3 | 1369 | 1836 |
| 25 | 549 | 6 | 544 | 0.15 | 0.058 | 0.0004 | 0.0023 | 1.50E−05 | 0.282377 | 1.80E−05 | 0.2824 | −2.7 | 1281 | 1678 |
| 26 | 552 | 7 | 470 | 0.10 | 0.063 | 0.0000 | 0.0024 | 2.90E−06 | 0.282398 | 2.00E−05 | 0.2824 | −2 | 1256 | 1633 |
| 27 | 544 | 6 | 342 | 0.57 | 0.054 | 0.0003 | 0.0021 | 9.20E−06 | 0.282447 | 1.90E−05 | 0.2824 | −0.3 | 1175 | 1521 |
| 28 | 528 | 6 | 516 | 0.11 | 0.034 | 0.0007 | 0.0014 | 2.60E−05 | 0.28234 | 2.20E−05 | 0.2823 | −4.1 | 1301 | 1751 |
| 29 | 543 | 6 | 596 | 0.13 | 0.063 | 0.0005 | 0.0025 | 1.90E−05 | 0.282326 | 2.50E−05 | 0.2823 | −4.7 | 1363 | 1800 |

Notes: zircon Lu-Hf isotopes were measured using a Nu plasma multi-collector ICP-MS equipped with a New Wave UP-213 laser-ablation system at the Institute of Earth Sciences, Academia Sinica, Taipei, Taiwan. Lu-Hf isotopic calculations are made with following equations:
$\lambda_{Lu\text{-}Hf} = 1.86 \times 10^{-11}$ y (Scherer et al., 2001).
$\varepsilon Hf(T) = [(^{176}Hf/^{177}Hf)^{T}_{Sample}/(^{176}Hf/^{177}Hf)^{T}_{CHUR} - 1] \times 10^{4}$ (Patchett and Tastumoto, 1981).
$(^{176}Hf/^{177}Hf)^{T}_{Sample} = (^{176}Hf/^{177}Hf)^{0}_{Sample} - (^{176}Lu/^{177}Hf)^{0}_{Sample} \times (e^{\lambda T} - 1)$; $(^{176}Hf/^{177}Hf)^{T}_{CHUR} = (^{176}Hf/^{177}Hf)^{0}_{CHUR} - (^{176}Lu/^{177}Hf)^{0}_{CHUR} \times (e^{\lambda T} - 1)$.
$(^{176}Hf/^{177}Hf)^{0}_{CHUR} = 0.282772$; $(^{176}Hf/^{177}Hf)^{0}_{CHUR} = 0.0332$ (Blichert-Toft and Albarède, 1997).
$(^{176}Hf/^{177}Hf)_{DM} = 0.28325$; $(^{176}Lu/^{177}Hf)_{DM} = 0.0384$ (Nowell et al., 1998; Griffin et al., 2000).
$(^{176}Lu/^{177}Hf)_{mean\ crust} = 0.015$ (Griffin et al., 2000).
$f_{CC} = (0.015/0.0332) - 1 = -0.5482$; $f_{DM} = (0.0384/0.0332) - 1 = 0.1566$.

The data of Bitlis gneisses and metagranites (Ustaömer et al., 2012) and Derik volcanics (Gürsu et al., 2015) were compared with our results from Pütürge gneisses in this study.

## 5. Whole-rock geochemistry

The augen gneisses of the Pütürge Massifs display similar range of compositions from tonalite to monzogranite with the rocks from Bitlis Massifs and Derik volcanics. The most common rocks are monzogranite (Fig. 5), and their $SiO_2$ content ranging from 57.3% to 71.6%. They contain 1.27–4.11% $K_2O$ and 1.53–5.28% $Na_2O$. Since the major element, and especially alkali elements, classification is dubious due to alteration of the Pütürge gneisses, immobile trace elements have been used to constrain their tectonic environment of formation.

Chondrite-normalized REE patterns of the augen gneisses -of Pütürge Massifs show similar trends with metagranites of Bitlis Massifs and volcanics of Derik. The augen gneisses of Pütürge Massif show an enrichment of LREE (light rare earth elements) in respect to HREE (heavy rare earth elements; LaN/YbN = 5.21–15.37) and relatively flat HREE (GdN/YbN = 1.55–2.02). (Fig. 6a and b). The nature of the negative Eu anomalies suggests that the rocks evolved by fractional crystallization of plagioclase or that they originated from partial melting in the presence of feldspar in the source.

In the primitive mantle-normalized incompatible element spidergrams (element ordering after Thompson et al., 1984), the augen gneisses of Pütürge Massif display overall LILEs (Large Ion Litophile Elements)-enriched patterns, with negative Nb, Ta, Sr, P, and Ti and positive Rb and Th anomalies (Fig. 6c and d).

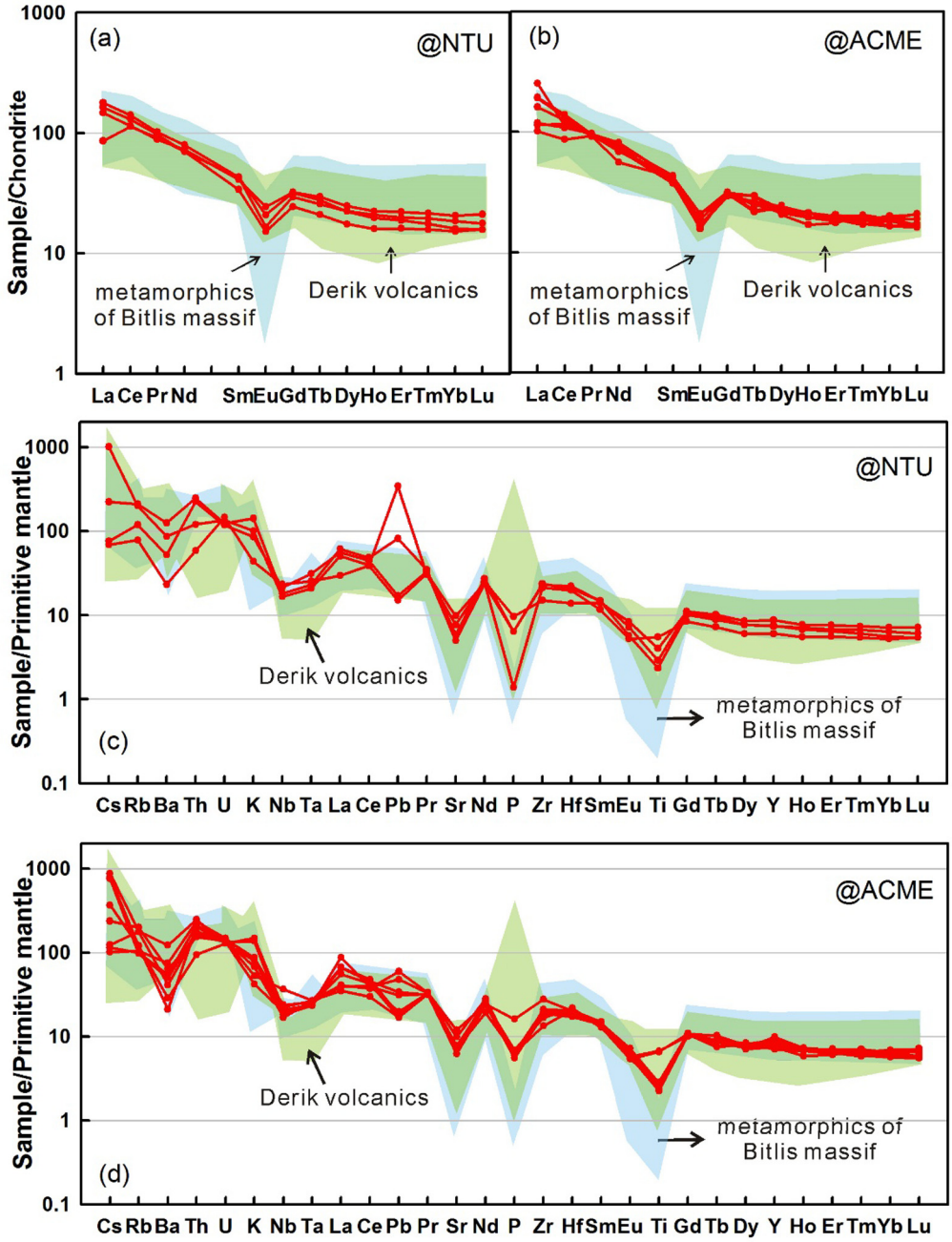


**Fig. 6.** (a and b) Chondrite-normalized REE patterns and (c and d) primitive mantle normalized spidergrams of Pütürge augen gneisses and metagranites. The blue area are the results of metamorphics of Bitlis massifs from Ustaömer et al. (2012); the green area are the results of Derik volcanics from Gürsu et al. (2015). Normalized values from Sun and McDonough (1989). (For interpretation of the references to color in this figure legend, the reader is referred to the web version of this article.)

Enrichment in Large Ion Lithophile Elements (LILEs) and depletion in High Field Strength Elements (HFSEs) suggest that these rocks originated above a subduction-related zone. Depletion in Ti and Sr could be related to the titanomagnetite and feldspar (with Eu anomaly) fractionation.

Based on Co vs Th of Hastie et al. (2007) diagram, they classify as high-K calc-alkaline alkaline and shoshonitic granites (Fig. 7a). In the discrimination diagrams for differentiated rocks, i.e., Zr vs. $Nb/Zr_{(n)}$ (ppm) diagram of Thiéblemont and Tegyey (1994), the augen gneisses of Pütürge Massif plot on the boundary between the subduction-related field and the collision-related field. However, rocks from Bitlis Massif and Derik plot within the subduction to collision-related fields. The other three discrimination diagrams for granites after Pearce et al. (1984), i.e., Yb vs. Ta, Y + Nb vs. Rb, and Yb + Ta vs. Rb, suggest that all the studied rocks were volcanic arc granites. On Schandl and Gorton (2002) diagrams (e.g., Th/Yb vs Ta/Yb) gneisses show characteristics of the volcanic rocks generated in active continental margin (ACM) (Fig. 7b and f).

## 6. Zircon U-Pb ages

Two samples from the Pütürge augen gneiss were selected for *in-situ* zircon U–Pb dating and Lu-Hf isotopic analysis. In CL

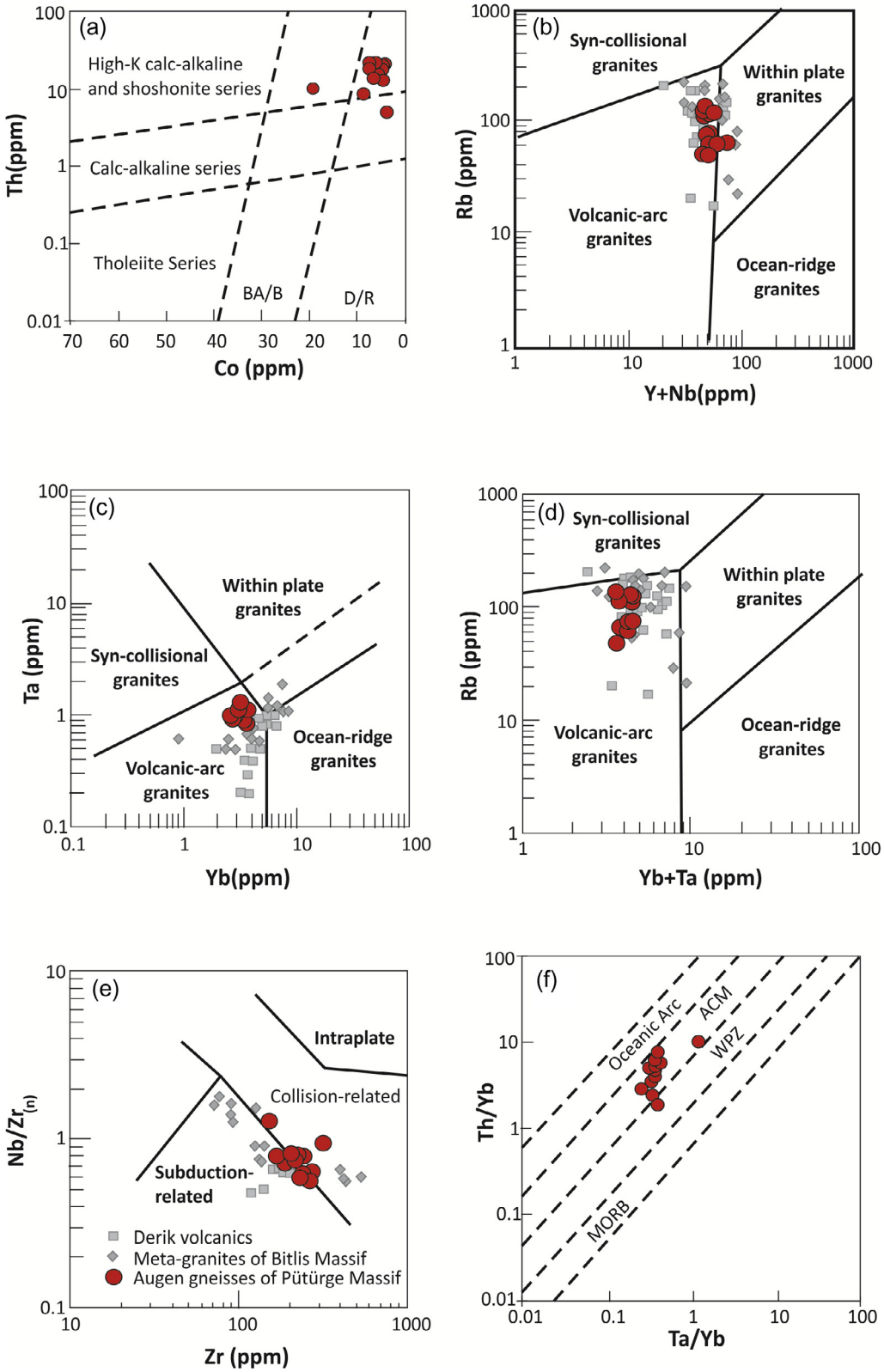


**Fig. 7.** (a) Discrimination diagram of differentiated lavas, Zr versus $Nb/Zr_{(n)}$ diagram after Thiéblemont and Tegyey, 1994; (b–d) Trace element discrimination diagrams of granitic rocks, Yb vs. Ta, (Y + Nb) vs. Rb, and (Yb + Ta) vs. Rb (ppm) diagrams after Pearce et al. (1984).

images, the zircons are mostly euhedral, colorless to pale brown, and show oscillatory zoning suggesting an igneous origin (Fig. 8). The augen gneiss samples of 13TK51 and 13TK54 show variable Th/U ratios of 0.08–0.87 and 0.09–0.57, respectively (Table 2). This high Th/U ratio is consistent with an igneous origin for the analyzed zircons. The $^{206}Pb/^{238}U$ ages of 13TK51 range from 573 to 529 Ma, having a weighted mean $^{206}Pb/^{238}U$ age of 551 ± 6 Ma (n = 21, MSWD = 3.7, Fig. 9a). The $^{206}Pb/^{238}U$ ages of 13TK54 range

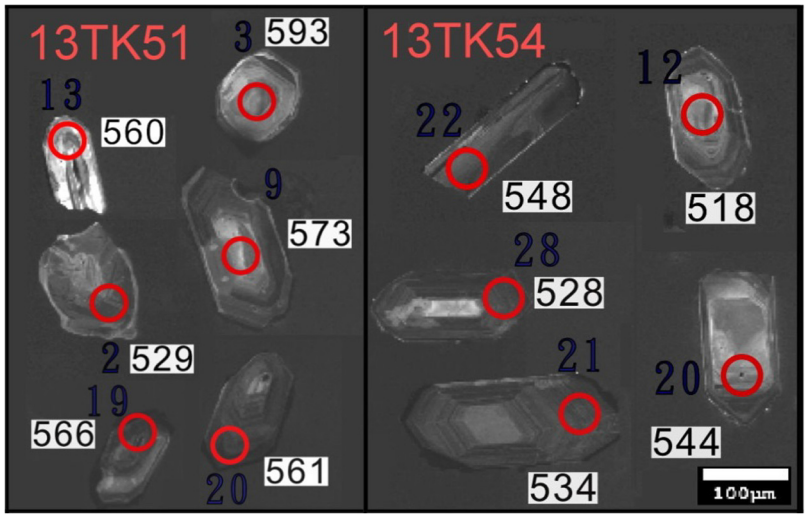


**Fig. 8.** Cathodoluminescence (CL) images and laser ablation ages for zircons from two Pütürge augen gneisses.

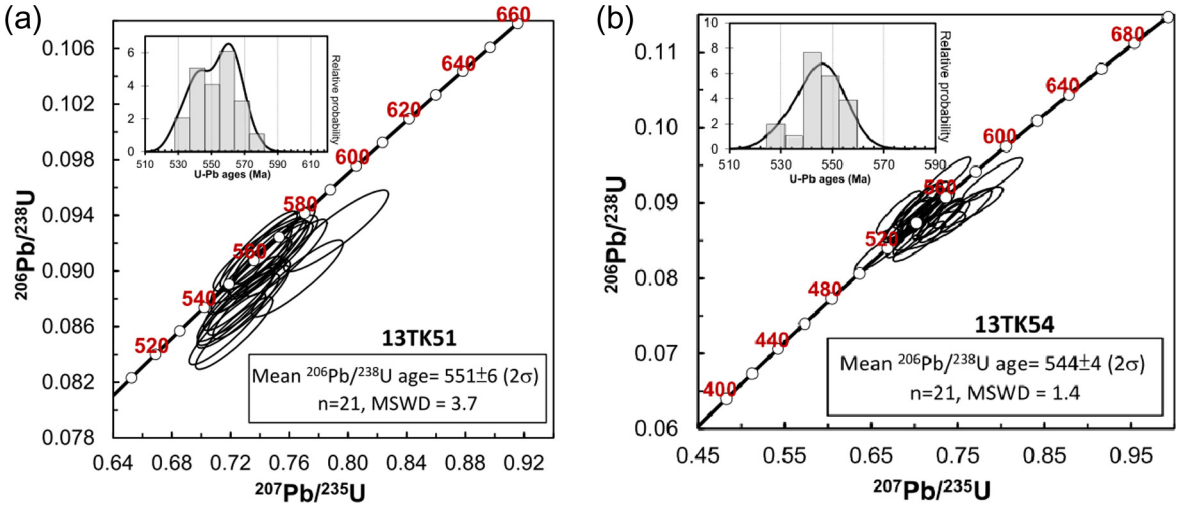


**Fig. 9.** U-Pb concordia plots and histograms of zircon U-Pb ages for two Pütürge augen gneiss: (a) 13TK51, (b) 13TK54.

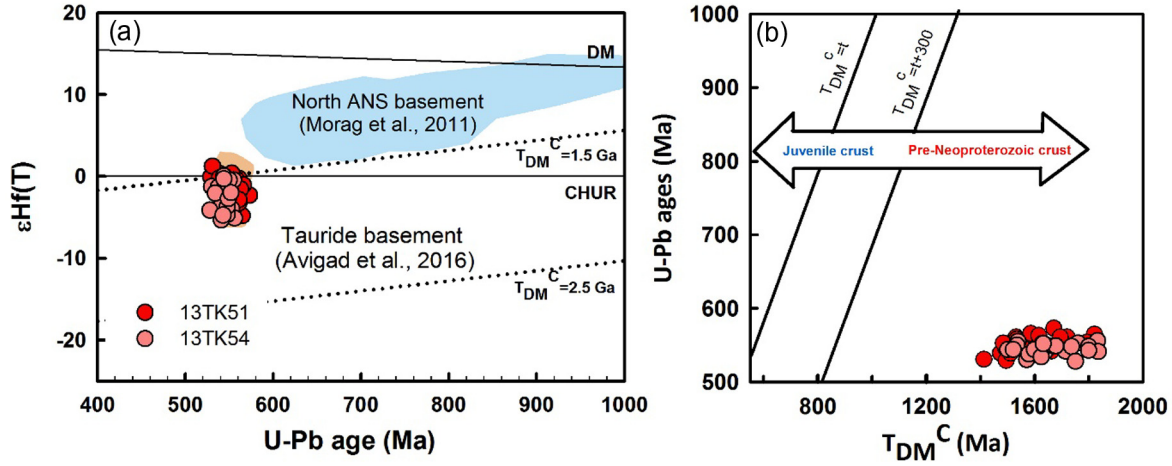


**Fig. 10.** (a) Zircon *in situ* U-Pb ages vs. εHf values and (b) U–Pb ages vs. $T_{DM}^{C}$ of two Pütürge augen gneisses.

from 556 to 528 Ma, having a weighted mean $^{206}Pb/^{238}U$ age of 544 ± 4 Ma (n = 21, MSWD = 1.4, Fig. 9b). These two ages interpreted the time of zircon crystallization.

Zircon *in-situ* Lu-Hf isotopes were also analyzed for two Pütürge augen gneiss samples in the same spots of U-Pb analysis. They have similar $^{176}Yb/^{177}Hf$ and $^{176}Lu/^{177}Hf$ values of 0.020–0.075 and 0.001–0.003 (Table 3). The $^{176}Lu/^{177}Hf$ values are close to or less than 0.002, indicating that there is no significant accumulation of radiogenic Hf after the formation of these zircons. The initial $^{176}Hf/^{177}Hf$ ratios for the Pütürge gneisses range from 0.2823 to 0.2825 (εHf (t) = −5.3 to +1.2) with the crustal model ages range from 1.8 to 1.4 Ga, suggesting involvement of older continental crust in magma genesis (Fig. 10a and b). The Hf isotopic composition of Pütürge augen gneiss is similar to the other Cadomian intrusions (Ustaömer et al., 2012; Zlatkin et al., 2013; Avigad et al., 2016) including the granites and metagranite from Bitlis Massif (εHf (t) = −2 to −1 and −5 to −4), the orthogneisses from Menderes Massif (εHf (t) = −5 to +2), and the igneous rocks from Tauride Massif (εHf (t) = −6 to +3).

## 7. Discussion

The geochemical data of the rocks in this study were plotted on various major and trace element tectonic discrimination diagrams. In the Co versus Th diagram of Hastie et al. (2007) (Fig. 7a), the augen gneisses of Pütürge Massif fall in the high-K calc-alkaline and shoshonitic field. The augen gneisses are compared with volcanic arc granite (VAG) syn-collision granite (syn-COLG), within plate granite (WPG) and orogenic related granite (ORG). In Y + Nb versus Rb, Ta versus Yb diagrams and Yb + Ta versus Rb of Pearce et al. (1984) (Fig. 7b–d), augen gneisses of Pütürge Massif fall in the volcanic arc granite (VAG) field; the subduction-related tectonic setting is also supported by the distinct negative Nb, Ta, P and Ti anomalies in primitive mantle normalized trace elements diagrams (Fig. 6c and d). In the Zr versus $Nb/Zr_n$ diagram (Fig. 7e), augen gneisses samples fall between the subduction-related field and the collision related field. In all diagrams, the Pütürge augen gneisses fall into the same fields with meta-granites of Bitlis Massif and Derik volcanics (Fig. 7b–e). Gorton and Schandl (2000) suggest a tectonic discrimination based on the concentrations and ratios between Th, Ta and Yb. In this classification, the Th/Ta values of the Pütürge augen gneiss samples (5–22.34, with an average of 14.52) are similar to those of felsic to intermediate volcanic rocks of active continental margins (Th/Ta between 6 and 20). In the Th/Ta versus Yb diagram idealized by Gorton and Schandl (2000), the samples plot mostly in the active continental margin field (Fig. 7f). In a similar manner, the La/Nb ratios of 1.07–4 (average 2.49) are remarkably within the range of those of arc magmas (1.3–6), in comparison to within-plate magmas in which this ratio is much lower (around 0.8; Rudnick, 1995).

The new zircon crystallization ages of 551 ± 6 Ma and 544 ± 4 Ma (Ediacaran–Early Cambrian) constitute the first U/Pb radiometric dates of augen gneisses from the Pütürge Massif in SE Turkey. The combined major-element, trace-element suggest the existence of Andean type arc-related magmatism.

Whereas zircon dating is crucial in identifying the protolith age for granitic rocks that were subjected to high-grade metamorphism, Hf isotopes can be used to determine the nature of the protolith (Zheng et al., 2004, 2006; Belousova et al., 2006; Wu et al., 2007). A depleted-mantle model age ($T_{DM}$) for the magmatic host rock of a given zircon is calculated using the measured $^{176}Hf/^{177}Hf$ and $^{176}Lu/^{177}Hf$ of the zircon. Calculation results give a minimum age for the source rock of the host magma. A more realistic "crustal" model age ($T^{C}_{DM}$) is calculated by assuming that the source rocks of the magma had the $^{176}Lu/^{177}Hf$ ratio of the average continental crust. Large differences in the Hf-isotope composition of zircon grains of similar age can be explained either by mixing crust- and mantle-derived magmas (Griffin et al., 2002; Belousova et al., 2006), or by melting of a heterogenous crustal sources (Ali et al., 2015). Zircon typically contains tens of ppm of Lu but ~1% Hf (Hiess et al., 2009), thus it is the major reservoir for Hf in granitoids (Hoskin and Schaltegger, 2003; Hiess et al., 2009). The very low $^{176}Lu/^{177}Hf$ ratios of zircons result in their present-day Hf isotopic compositions approximating that of magmas from which the zircons crystallized (Kinny and Maas, 2003). These zircons have $^{176}Hf/^{177}Hf$ ratios consistent with evolution in a reservoir with $^{176}Lu/^{177}Hf$, i.e. continental crust (low $^{176}Lu/^{177}Hf$) or depleted mantle (high $^{176}Lu/^{177}Hf$), or reflect a mixture of melts from older crust and depleted mantle (Amelin et al., 2000; Chauvel and Blichert-Toft, 2001; Hiess et al., 2009). The Pütürge gneissic rocks yielded $\varepsilon Hf_{(t)}$ values of −5.3 to +1.2) with the crustal model ages range from 1.8 to 1.4 Ga, suggesting involvement of older continental crust in magma genesis. The elemental variations from our study reveal that the studied rocks may have been derived from crust-derived (lower crustal) magmas and followed by limited effects of the assimilation-fractional crystallization (AFC) process of the middle and/or upper continental crustal source. Their negative εHf(t) and older TDM ages are clearly restricted a juvenile mafic source. On the primitive mantle normalized multi-element diagrams, augen gneisses display relative enrichment in HFSE and REE and indicate that they may have been derived from mafic lower continental crustal sources followed by mixing of middle or upper continental crustal materials during the magma emplacement.

The crustal modal ages varying from 1.4 to 1.8 Ga in augen gneisses are older than U–Pb crystallization age of the studied samples and show either a contamination of the lower crustal source with older material or older source.

Our new results can also be compared with previous evidence of dated Late Precambrian-Early Cambrian magmatic rocks in Turkey and in Iran. The nearest of these units to the Pütürge gneisses are the Ediacaran–Early Cambrian meta-granites in Bitlis Massif. Ustaömer et al. (2009, 2012) obtained a $^{207}Pb/^{206}Pb$ single-zircon age of 545.5 ± 6.1 Ma and 531.4 ± 3.6 Ma from Mutki meta-granites and an age of 572 ± 4.8 Ma from Doğanyol meta-granites in the Bitlis Massif. The Mutki granite yielded $\varepsilon_{Nd(t=545)}$ values of −1.88 and −1.237, whereas granitic dikes yielded $\varepsilon_{Nd(t=532)}$ values of −2.88 and −2.03 (Ustaömer et al., 2009), for which a TDM (Nd) model age of 1.3 Ga was estimated. Doğruyol meta-granite yielded $\varepsilon_{Nd(t=567)}$ of −5.13 and −4.11 (Ustaömer et al., 2012). The $^{206}Pb/^{238}U$ crystallization ages of the meta-granitic intrusions within the high-grade metamorphic basement of the central and the southern Menderes Massif show that they were formed during the Late Neoproterozoic, between 543 and 554 Ma (Hetzel and Reischmann, 1996; Oberhänsli et al., 1998, 2010; Loos and Reischmann, 1999, 2001; Gessner et al., 2004; Candan et al., 2001, 2011; Koralay et al., 2012; Gürsu, 2016). These Cadomian igneous rocks yielded $\varepsilon_{Hf(t)}$ values of −5 and +2 with corresponding Hf depleted mantle model ages (Hf-$T_{DM}$) of 1.2–1.6 Ga (Zlatkin et al., 2013; Avigad et al., 2016). Cadomian late to post-collisional I-type granitic rocks mainly intruded Tauride-Anatolite Platform (N and S of Afyon) and were cut by abundant tholeiitic dikes between 560 and 545 Ma (Gürsu and Göncüoğlu, 2005, 2008) and South Anatolian Autochthone Belt (Derik volcanics) (Gürsu et al., 2015). The Derik volcanics have 581 ± 4 Ma and 559 ± 3 Ma for the early and late-stage andesitic rocks, 570 ± 2 Ma, 572 ± 2 Ma, and 575 ± 4 Ma for the rhyolites (Gürsu et al., 2015).

The granitoids of the Cadomian Orogeny can be traced eastward into Iran, Central Iran (ca. 599–525 Ma, Ramezani and Tucker, 2003; Hassanzadeh et al., 2008; Moghadam et al., 2015), the

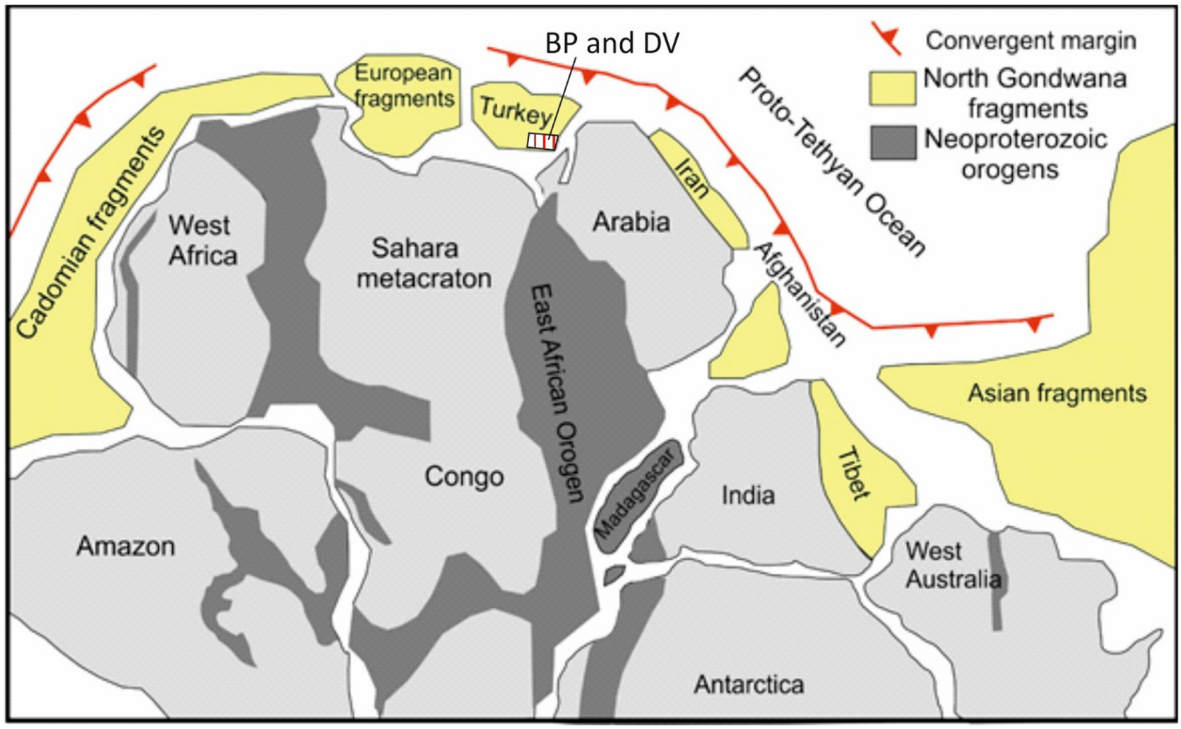


**Fig. 11.** Map of a part of Gondwana, showing the position of the continents and smaller continental fragments in the early Mesozoic (modified after Moghadam et al., 2015).

Sanandaj-Sirjan Zone (ca. 596–540 Ma, Hassanzadeh et al., 2008; Jamshidi Badr et al., 2013; Moghadam et al., 2015). U-Pb zircon geochronology of various orthogneiss in Turkey and in Iran Neoproterozoic basement yielded ~599–525 Ma ages. A cumulative zircon U-Pb ages of all available data for Cadomian igneous rocks of the Turkey and Iran defines a concentration in a narrow time interval about 550 Ma (Yılmaz-Şahin et al., 2014; Moghadam et al., 2015; Avigad et al., 2016).

Hf and Nd isotopic data and the nagative $\varepsilon_{Hf(t)}$ and $\varepsilon_{Nd}$ values from Cadomian-Early Cambrian igneous rocks of the Turkey, except Derik volcanics, and Iran thus indicate the involvement of preexisting crust in their generation, with Hf model ages of 1.2–1.8 Ga. Gürsu et al. (2015) suggest that the average positive εNd (T) data of the Derik volcanik indicate that early-stage andesites and mafic dykes were dominantly generated from subduction-enriched mantle-derived magmas but rhyolites and late-stage andesites have lower positive εNd(T) values than early-stage andesites and mafic dykes and clearly indicate the effects of contamination with crustal source in their genesis. There are many Cadomian-Avolian Terranes in Europe, in Asia and in America (Fig. 11). There is indeed general agreement that an active Andean-type continental margin, featuring magmatic arcs and back-arc basins, formed the entire northern margin of Gondwana, with subduction beginning at about 760 Ma and ending diachronously with the development of transform fault systems (e.g. Neubauer, 2002; Stampfli et al., 2002; Von Raumer et al., 2002; Murphy et al., 2004). The Neoproterozoic-Cambrian time frame was dominated by the growth of the Gondwana Supercontinent that resulted from a long-lived history of orogenic construction, starting from the breakup of Rodinia (870–800 Ma) to the final amalgamation in Cambrian times (e.g. Dalziel, 1991; Meert, 2003; Boger and Miller, 2004; Collins and Pisarevsky, 2005; Cawood, 2005; Cawood and Buchan, 2007; Li et al., 2008; Torsvik and Cocks, 2013; Nance et al., 2014). The terminal assembly of Gondwana largely occurred older than or about 600 Ma and was achieved through accretion of various continental blocks both involving prolonged collisional assembly of East and West Gondwana continents (Meert, 2003; Collins and Pisarevsky, 2005; Meert and Lieberman, 2008) and development of subduction systems all along the margins of the Gondwana supercontinent (Terra Australis Orogen and North India Orogen, Boger and Miller, 2004; Cawood, 2005; Cawood et al., 2007; Murphy et al., 2011). The assembly of the Gondwana supercontinent during the late Neoproterozoic involved closure of the intervening Neoproterozoic oceans (Collins et al., 2007) and subduction of a substantial volume of oceanic lithosphere along a number of convergent margins (Santosh et al., 2009). Prior to the breakup, the Gondwana supercontinent had an active subduction margin along the Pacific side (Cawood, 2005), whereas on the northern side there was a passive margin (Windley, 1992; Şengör, 1984). This passive margin also occurred in Iran (Moghadam et al., 2015), and in Turkey. In Turkey, the Cadomian fragments mainly occured in three separate Alpine tectonic units; the Istanbul-Zonguldak Zone (Bolu Massif, 576–565 Ma, Chen et al., 2002; Ustaömer et al., 2005), the Tauride–Anatolian Block (570–540 Ma, Gürsu et al., 2004; Gessner et al., 2004; Gürsu and Göncüoglu, 2006; Candan et al., 2015), the Bitlis Massif of SE Turkey (545–531 Ma from Ustaömer et al., 2009 and 572 Ma from Ustaömer et al., 2012), Pütürge augen gneisses of SE Turkey (551–544 Ma, this study) and South Anatolian Autochthone Belt (Derik volcanics, Gürsu et al., 2015).

Subduction of Proto-Tethys oceanic lithosphere beneath the Gondwana was responsible for arc magmatism at the northern edge of Gondwana during the Late Proterozoic to Early Cambrian (Ramezani and Tucker, 2003; Nadimi, 2007). Subduction beneath the active margin of Gondwana is suggested to have ceased around 450–400 Ma, due to continental or oceanic plateau collision (Ustaömer et al., 2009). After this collision, Ordovician rifting opened Paleotethys, separating slices of N Gondwana from the Southeast Anatolian Massifs (Bitlis-Pütürge) and Derik volcanics and they were re-amalgamated in Oligo-Miocene times. The basement rocks of the Bitlis-Pürtürge Massifs were strongly deformed and metamorphosed under amphibolite facies conditions, but

eclogite relicts are also present during the Cadomian orogeny. Metamorphic domains in zircon crystals seem to date the last Cadomian metamorphism (529 ± 5 Ma, Ustaömer et al., 2012). This was possibly related to a collision during the final amalgamation of exotic terranes with northeast Gondwana, or to the development of a subsequent subduction zone along the margin Gondwana (Collins and Pisarevsky, 2005).

## 8. Conclusion

Augen gneisses and metagranites of the Bitlis-Pütürge Massifs and non-metamorphic Derik volcanics have late Neoproterozoic (Ediacaran) to early Cambrian (Terreneuvien) ages. They show geochemical characteristics suggesting an origin from active margin magmatism that we infer to have occurred in the northern margin of Gondwana. In this study, we report for the first time zircon U-Pb ages (551 ± 6 and 544 ± 4 Ma) of two augen gneisses form the Pütürge Massif. Zircon εHf(t) values of these augen gneisses suggest the involvement of older continental crust in magma genesis. The Hf model ages suggest that this older crust is of the Mesoproterozoic, ~1.4–1.8 Ga. Augen gneisses and meta-granites of the Bitlis-Pütürge Massifs. Together with the Derik volcanics and other coeval basement rocks in the Tauride–Anatolian block (Turkey) were part of Gondwana until the Paleozoic, when they separated during Neotethys rifting and then were re-amalgamated in Oligo-Miocene times. The high grade metamorphism of the Lower units of the Bitlis-Pütürge Massifs was possibly related to a collision during the final amalgamation of exotic terranes with northeast Gondwana, or to the development of a subsequent subduction zone along the margin of Gondwana.

## Acknowledgments

We thank Mustafa Rizeli and Mehmet ERTURK (Firat University) for field assistance, and Chien-Huei Hung, Hao-Yang Lee and Te-Hsien Lin (National Taiwan University) for laboratory assistance. This study was performed under a joint research program supported by Firat University – Turkey and National Taiwan University – Taiwan. The authors are greatly appreciated to editor and two reviewers for contributions and recommendations that significantly improved the manuscript.

## References

Aktaş, G., Robertson, H.F., 1984. The Maden Complex, SE Turkey: evolution of a Neotethyan active margin. In: Dixon, J.E., Robertson, A.H.F. (Eds.), The Geological Evolution of the Eastern Mediterranean. The Geological Society by Blackwell Scientific Publication, Oxford, London, Edinburgh, Boston, Palo Alto, Melbourne, pp. 375–401.

Ali, K.A., Basem, A., Zoheir, B.A., Stern, R.J., Andresen, A., Whitehouse, M.J., Bishara, W.W., 2015. Lu–Hf and O isotopic compositions on single zircons from the North Eastern Desert of Egypt, Arabian-Nubian Shield: implications for crustal evolution. Gondwana Res. http://dx.doi.org/10.1016/j.gr.2015.02.008.

Amelin, Y.V., Lee, D.C., Halliday, A.N., 2000. Early-Middle Archaean crustal evolution deduced from Lu-Hf and U-Pb isotopic studies of single zircon grains. Geochim. Cosmochim. Acta 64, 4205–4225.

Avigad, D., Abbo, A., Gerdes, A., 2016. Origin of the Eastern Mediterranean: Neotethys rifting along a cryptic Cadomian suture with Afro-Arabia. Geol. Soc. Am. Bull. http://dx.doi.org/10.1130/B31370.1.

Belousova, E.A., Griffin, W.L., O'Reilly, S.Y., 2006. Zircon crystalmorphology, trace element signatures and Hf isotope composition as a tool for petrogenetic modelling: examples from eastern Australian granitoids. J. Petrol. 47, 329–353.

Blichert-Toft, J., Albarède, F., 1997. The Lu-Hf isotope geochemistry of chondrites and the evolution of the mantle-crust system. Earth Planet. Sci. Lett. 148 (1), 243–258.

Boger, S.D., Miller, J.M., 2004. Terminal suturing of Gondwana and the onset of the Ross–Delamerian Orogeny: the cause and effect of an Early Cambrian reconfiguration of plate motions. Earth Planet. Sci. Lett. 219, 35–48.

Candan, O., Dora, O., Oberhansli, R., Cetinkaplan, M., Partzsch, J., Warkus, F., Durr, S., 2001. Pan-African high-pressure metamorphism in the Precambrian basement of the Menderes Massif, western Anatolia, Turkey. Int. J. Earth Sci. 89 (4), 793.

Candan, O., Koralay, O.E., Akal, C., Kaya, O., Oberhänsli, R., Dora, O.Ö., Konak, N., Chen, F., 2011. Supra-Pan-African unconformity between core and cover series of the Menderes Massif/Turkey and its geological implications. Precambr. Res. 184, 1–23.

Candan, O., Koralay, O.E., Topuz, G., Oberhansli, R., Fritz, H., Collins, A.S., Chen, F., 2015. Late Neoproterozoic gabbro emplacement followed by early Cambrian eclogite-facies metamorphism in the Menderes Massif (W. Turkey): implications on the final assembly of Gondwana. Gondwana Res. http://dx.doi.org/10.1016/j.gr.2015.02.015.

Cawood, P.A., 2005. Terra Australis Orogen. Rodinia breakup and development of the Pacific and Iapetus margins of Gondwana during the Neoproterozoic and Paleozoic. Earth-Sci. Rev. 69, 249–279.

Cawood, P.A., Buchan, C., 2007. Linking accretionary orogenesis with supercontinent assembly. Earth-Sci. Rev. 85, 217–256.

Cawood, P.A., Johnson, M.R.W., Nemchin, A.A., 2007. Early Palaeozoic orogenesis along the Indian margin of Gondwana. Tectonic response to Gondwana assembly. Earth Planet. Sci. Lett. 255, 1–2 (15, 70–84).

Chauvel, C., Blichert-Toft, J., 2001. A hafnium isotope and trace element perspective on melting of the depleted mantle. Earth Planet. Sci. Lett. 190, 137–151.

Chen, F., Siebel, W., Satir, M., Terzioğlu, M.N., 2002. Geochronology of the Karadere basement (NW Turkey) and implications for the geological evolution of the Istanbul zone. Int. J. Earth Sci. 91, 469–481.

Chiu, H.-Y., Chung, S.-L., Wu, F.-Y., Liu, D., Liang, Y.-H., Lin, I.-J., Iizuka, Y., Xie, L.-W., Wang, Y., Chu, M.-F., 2009. Zircon U-Pb and Hf isotopic constraints from eastern Transhimalayan batholiths on the precollisional magmatic and tectonic evolution in southern Tibet. Tectonophysics 477 (1), 3–19.

Cocks, L.R.M., Torsvik, T.H., 2011. The Palaeozoic geography of Laurentia and western Laurussia: a stable craton with mobile margins. Earth-Sci. Rev. 106, 1–51.

Collins, A.S., Pisarevsky, S.A., 2005. Amalgamating eastern Gondwana: the evolution of the Circum-Indian Orogens. Earth-Sci. Rev. 71, 229–270.

Collins, A.S., Clark, C., Sajeev, K., Santosh, M., Kelsey, D.E., Hand, M., 2007. Passage through India: the Mozambique Ocean suture, high-pressure granulites and the Palghat-Cauvery shear zone system. Terra Nova 19, 141–147.

Dalziel, I.W.D., 1991. Pacific margins of Laurentia and East Antarctica-Australia as a conjugate rift pair: evidence and implications for an Eocambrian supercontinent. Geology 19, 598–601.

Erdem, E., 1994. Pütürge (Malatya) Metamorphitlerinin petrografik ve petrolojik özellikleri Ph.D. Thesis. Firat Univ. Inst. of Sciences and Technology, Elazığ, Turkey, 119p. (in Turkish).

Erdem, E., Bingöl, A.F., 1995. Pütürge (Malatya) Metamorfitlerinin Petrografik Özellikleri. F.Ü.Fen ve Müh. Bilimleri Dergisi 7 (1), 73–85 (in Turkish).

Fernandez-Suarez, J., Guitierrez-Alonso, G., Jenner, G.A., Tubrett, M.N., 2000. New ideas on the Proterozoic–early Palaeozoic evolution of NW Iberia; insights from U-Pb detrital zircon ages. Precambr. Res. 102, 185–206.

Fernandez-Suarez, J., Gutierrez-Alonso, G., Jeffries, T.E., 2002. The importance of along margin terrane transport in northern Gondwana: insights from detrital zircon parentage in Neoproterozoic rocks from Iberia and Brittany. Earth Planet. Sci. Lett. 204, 75–88.

Gessner, K., Collins, A.S., Ring, U., Güngör, T., 2004. Structural and thermal history of poly-orogenic basement: U-Pb geochronology of granite rocks in the southern Menderes Massif, Western Turkey. J. Geol. Soc. 161, 93–101.

Ghienne, J.F., Monod, O., Kozlu, H., Dean, W.T., 2010. Cambrian-Ordovician depositional sequences in the Middle East: a perspective from Turkey. Earth Sci. Rev. 101, 101–146.

Göncüoğlu, M.C., Turhan, N., 1984. Geology of the Bitlis Metamorphic Belt. In: Tekeli, O., Göncüoğlu, M.C. (Eds.), International Symposium on Geology of the Taurus Belt Proceedings. Mineral Research and Exploration Institute of Turkey, Ankara, pp. 237–244.

Göncüoglu, M.C., Kozlu, H., 2000. Early Palaeozoic evolution of the NW Gondwanaland: data from southern Turkey and surrounding regions. Gondwana Res. 3, 315–323.

Gorton, M.P., Schandl, E.S., 2000. From continents to island arcs: A geochemical index of tectonic setting for arc-related and within-plate felsic to intermediate volcanic rocks. Can. Mineral. 38, 1065–1073.

Griffin, W.L., Pearson, N.J., Belousova, E., Jackson, S.E., van Achterbergh, E., O'Reilly, S.Y., Shee, S.R., 2000. The Hf isotope composition of cratonic mantle: LAM-MC-ICPMS analysis of zircon megacrysts in kimberlites. Geochim. Cosmochim. Acta 64, 133–147.

Griffin, W.L., Wang, X., Jackson, S.E., Pearson, N.J., O'Reilly, S.Y., Xu, X., Zhou, X., 2002. Zircon chemistry and magma mixing SE China: in-situ analysis of Hf isotopes, Tonglu and Pingtan igneous complexes. Lithos 61, 237–269.

Gürsu, S., 2016. A new petrogenetic model for meta-granitic rocks in the central and southern Menderes Massif – W Turkey: implications for Cadomian crustal evolution within the Pan-African mega-cycle. Precambr. Res. 275, 450–470.

Gürsu, S., Göncüoğlu, M.C., 2005. Early Cambrian back-arc volcanism in the western Taurides, Turkey: implications for rifting along the northern Gondwanan margin. Geol. Mag. 142 (5), 617–631. http://dx.doi.org/10.1017/S0016756805000919.

Gürsu, S., Göncüoğlu, M.C., 2006. Petrogenesis and tectonic setting of Cadomian felsic igneous rocks, Sandıklı area of the western Taurides, Turkey. Int. J. Earth Sci. 95, 741–757.

Gürsu, S., Göncüoğlu, M.C., 2008. Petrogenesis and geodynamic evolution of the late Neoproterozoic post-collisional felsic magmatism in NE Afyon area, western central Turkey. In: Ennih, N., Liegeios, J.P. (Eds.), The Boundaries of the West

African Craton. Geological Society of London Special Publication 297, pp. 409–431. http://dx.doi.org/10.1144/SP297.19.
Gürsu, S., Göncüoglu, M.C., Bayhan, H., 2004. Geology and geochemistry of the pre-Early Cambrian rocks in Sandıklı area: implications for the Pan-African evolution in NW Gondwanaland. Gondwana Res. 7, 923–935.
Gürsu, S., Möller, A., Göncüoglu, M.C., Köksal, S., Demircan, H., Toksoy Köksal, F., Kozlu, H., Sunal, G., 2015. Neoproterozoic continental arc volcanism at the northern edge of the Arabian Plate, SE Turkey. Precambr. Res. 258, 208–233.
Hassanzadeh, J., Stockli, D.F., Horton, B.K., Axen, G.J., Stockli, L.D., Grove, M., Schmitt, A.K., Walker, J.D., 2008. U-Pb zircon geochronology of late Neoproterozoic-Early Cambrian granitoids in Iran: implications for paleogeography, magmatism, and exhumation history of Iranian basement. Tectonophysics 451, 71–96. http://dx.doi.org/10.1016/j.tecto.2007.11.062.
Hastie, A.R., Kerr, A.C., Pearce, J.A., Mitchell, S.F., 2007. Classification of altered island arc rocks using immobile trace elements: development of the Th–Co discrimination diagram. J. Petrol. 48, 2341–2357.
Hetzel, R., Reischmann, T., 1996. Intrusion age of Pan-African augen gneisses in the southern Menderes Massif and the age of cooling after Alpine ductile extensional deformation. Geol. Mag. 133, 565–572.
Hiess, J., Bennetty, V.C., Nutman, A.P., Williams, I.S., 2009. In situ U-Pb, O and Hf isotopic compositions of zircon and olivine from Eoarchacan rocks, West Greenland: new insights to making old crust. Geochim. Cosmochim. Acta 73, 4489–4516.
Hoskin, P.W.O., Schaltegger, U., 2003. The composition of zircon and igneous and metamorphic petrogenesis. Rev. Mineral. Geochem. 53, 27–62.
Jamshidi Badr, M., Collins, A.S., Masoudi, F., Cox, G., Mohajjel, M., 2013. The U-Pb age, geochemistry and tectonic significance of granitoids in the Soursat Complex, Northwest Iran. Turk. J. Earth Sci. 21. http://dx.doi.org/10.3906/yer-1001-37.
Kellogg, H.E., 1960. Stratigraphic report, Derik-Mardin area. T.C. Petrol Işleri Genel Müdürlüğü Teknik Arşivi 126, 1–34 (in Turkish).
Keppie, J.D., Nance, R.D., Murphy, J.B., Dostal, J., 2003. Tethyan, Mediterranean, and Pacific analogues for the Neoproterozoic-Paleozoic birth and development of the peri Gondwanan terranes and their transfer to Laurentia and Laurussia. Tectonophysics 365, 195–219.
Ketin, İ., 1966. Güneydoğu Anadolunun Kambriyen teşekkülleri ve bunların Doğu Iran Kambriyeni ile mukayesesi. MTA Bull. 66, 75–87 (in Turkish with English abstract).
Kinny, P.D., Maas, R., 2003. Lu–Hf and Sm–Nd isotope systems in zircon. Rev. Mineral. Geochem. 53 (1), 327–341.
Koralay, E.O., Candan, O., Chen, F., Akal, C., Oberhänsli, R., Satır, M., Dora, O.Ö., 2012. Pan-African magmatism in the Menderes Massif: geochronological data from leucocratic tourmaline orthogneisses in western Turkey. Int. J. Earth Sci. 101, 2055–2081.
Li, Z.X., Bogdanova, S.V., Collins, A.S., Davidson, A., De Waele, B., Ernst, R.E., Fitzsimons, I.C.W., Fuck, R.A., Gladkochub, D.P., Jacobs, J., Karlstrom, K.E., Lu, S., Natapov, L.M., Pease, V., Pisarevsky, S.A., Thrane, K., Vernikovsky, V., 2008. Assembly, configuration, and break-up history of Rodinia. A synthesis. Precambr. Res. 160, 179–210.
Lin, I.-J., Chung, S.-L., Chu, C.-H., Lee, H.-Y., Gallet, S., Wu, G., Ji, J., Zhang, Y., 2012. Geochemical and Sr–Nd isotopic characteristics of Cretaceous to Paleocene granitoids and volcanic rocks, SE Tibet: petrogenesis and tectonic implications. J. Asian Earth Sci. 53, 131–150.
Linnemann, U., Nance, D.R., Kraft, P., Zulauf, G., 2007. The Evolution of the Rheic Ocean: From Avalonian-Cadomian Active Margin to Alleghenian-Variscan Collision. Geological Society of America Special Publication 423, 620 pp.
Loos, S., Reischmann, T., 1999. The evolution of the southern Menderes Massif in SW Turkey as revealed by zircon dating. J. Geol. Soc. 156, 1021–1030.
Loos, St., Reischmann, T., 2001. Discussion on the evolution of the southern Menderes Massif in SW Turkey as revealed by zircon dating. J. Geol. Soc. Lond. 158, 393–395.
Meert, J.G., 2003. A synopsis of events related to the assembly of eastern Gondwana. Tectonophysics 362, 1–40.
Meert, J.G., Lieberman, B.S., 2008. The Neoproterozoic assembly of Gondwana and its relationship to the Ediacaran-Cambrian radiation. Gondwana Res. 14, 5–21.
Michard, A., Whitechurch, H., Ricou, L.E., Montigny, R., Yazgan, E., 1984. Tauric subduction (Malatya-Elazığ Provinces) and its bearing on tectonics of the Tethyan realm in Turkey. In: Dixon, J.E., Robertson, A.H.F. (Eds.), The Geological Evolution of the Eastern Mediterranean, vol. 17. Geological Society of London, Special Publication, pp. 361–374.
Moghadam, H.S., Khademi, M., Hu, Z., Stern, Robert J., Santos, R.J., Wu, Y., 2015. Cadomian (Ediacaran–Cambrian) arc magmatism in the ChahJam–Biarjmand metamorphic complex (Iran): magmatism along the northern active margin of Gondwana. Gondwana Res. 27, 439–452.
MTA, 2004. Türkiye'nin 1/500.000 ölçekli haritası. Ankara.
Murphy, J.B., Fernández-Suárez, J., Keppie, J.D., Jeffries, T.E., 2004. Contiguous rather than discrete Paleozoic histories for the Avalon and Meguma terranes based on detrital zircon data. Bull. Geol. Soc. Am. 32 (7), 585–588.
Murphy, J.B., Cousens, B.L., Braid, J.A., Strachan, R.A., Dostal, J., Keppie, J.D., Nance, R. D., 2011. Highly depleted oceanic lithosphere in the Rheic Ocean: implications for Paleozoic plate reconstructions. Lithos 123, 165–175.
Nadimi, A., 2007. Evolution of the Central Iranian basement. Gondwana Res. 12, 324–333.
Nance, R.D., Murphy, J.B., 1996. Basement isotopic signatures and Neoproterozoic paleogeography of Avalonian-Cadomian and related terranes in the Circum-North Atlantic. Geol. Soc. Am. Spec. Pap. 304, 333–346.
Nance, R.D., Murphy, J.B., Keppie, J.D., O'Brien, S.J., 2002. A Cordilleran model for the evolution of Avalonia. Tectonophysics 352, 11–31.
Nance, R.D., Murphy, J.B., Strachan, R.A., Keppie, J.D., Gutiérrez-Alonzo, G., Fernández- Suárez, J., Quésada, C., Linnemann, U., D'Lemos, R., Pisarevsky, S. A., 2008. Neoproterozoic–Early Palaeozoic Tectonostratigraphy and Palaeogeography of the Peri-Gondwanan Terranes: Amazonian V. West African Connections. Special Publications 297, Geological Society of London, pp. 345–383.
Nance, R.D., Murphy, J.B., Santosh, M., 2014. The supercontinent cycle: a retrospective essay. Gondwana Res. 25, 4–29.
Neubauer, F., 2002. Evolution of late Neoproterozoic to early Palaeozoic tectonic elements in Central and Southeast European Alpine mountain belts: review and synthesis. Tectonophysics 352, 87–103.
Nowell, G.M., Kempton, P.D., Noble, S.R., Fitton, J.G., Saunders, A.D., Mahoney, J.J., Taylor, R.N., 1998. High precision Hf isotopic measurements of MORB and OIB by thermal ionization mass spectrometry into the depleted mantle. Chem. Geol. 149, 211–233.
Oberhänsli, R., Monie, P., Candan, O., Warkus, F.C., Partsch, J.H., Dora, O.O., 1998. The age of blueschist metamorphism in the Mesozoic cover series of the Menderes Massif. Schweiz. Mineral. Petrogr. Mitt. 78, 309alogi.
Oberhänsli, R., Candan, O., Bousquet, R., Rimmele, G., Okay, A.I., Goff, J., 2010. Alpine HP evolution of the eastern Bitlis complex, SE Turkey. In: Sosson, M., Kaymakci, N., Stephenson, R., Strarostenko, V., Bergerat, F. (Eds.), Sedimentary Basins, Tectonics from Black Sea an Caucasus to the Arabian Platform. Geological Society, London, Special Publications 340, p. 461.
Oberhänsli, R., Bousquet, R., Candan, O., Okay, A., 2012. Dating subduction events in East Anatolia, Turkey. Turk. J. Earth Sci. 21, 1–17.
Okay, A.I., Nikishin, A.M., 2015. Tectonic evolution of the southern margin of Laurasia in the Black Sea region. Int. Geol. Rev. 57 (5–8), 1051–1076. http://dx.doi.org/10.1080/00206814.2015.1010609.
Okay, A.I., Arman, M.B., Göncüoğlu, M.C., 1985. Petrology and phase relations of the kyanite-eclogites from Eastern Turkey. Contrib. Mineral. Petr. 91, 196–204.
Patchett, P.J., Tastumoto, M., 1981. Lu/Hf in chondrites and definition of a chondritic hafnium growth curve. Lunar Planet. Sci. XII Part 2, 822–824.
Pearce, J.A., Harris, N.B., Tindle, A.G., 1984. Trace element discrimination diagrams for the tectonic interpretation of granitic rocks. J. Petrol. 25 (4), 956–983.
Perinçek, D., 1980. Bitlis Metamorfitlerinde Volkanitli Triyas. Türkiye Jeoloji Kurumu Bülteni C.23, 201–211. Ağustos 1980.
Perinçek, D., Özkaya, I., 1981. Arabistan Kıtası Kuzey Kenarının Tektonik Evrimi. H. Ü. Yerbilimleri Derg. 8, 91–101.
Ramezani, J., Tucker, R.D., 2003. The Saghand Region, Central Iran: U-Pb geochronology, petrogenesis and implications for Gondwana tectonics. Am. J. Sci. 303, 622–665.
Rudnick, R.L., 1985. Making continental crust. Nature 378, 571–577.
Santosh, M., Maruyama, S., Sato, K., 2009. Anatomy of a Cambrian suture in Gondwana: Pacific-type orogeny in southern India? Gondwana Res. 16, 321–341.
Schandl, E.S., Gorton, M.P., 2002. Application of high field strength elements to discriminate tectonic setting in VMS environments. Econ. Geol. 97, 629–642.
Scherer, E., Münker, C., Mezger, K., 2001. Calibration of the lutetium–hafnium clock. Science 293, 683–687.
Shao, W.-Y., Chung, S.-L., Chen, W.-S., Lee, H.-Y., Xie, L., 2015. Old continental zircons from a young oceanic arc, eastern Taiwan: implications for Luzon subduction initiation and Asian accretionary orogeny. Geology 43, 479–482.
Stampfli, G.M., 2000. Tethyan oceans. In: Bozkurt, E., Winchester, J.A., Piper, J.D. (Eds.), Tectonics and Magmatism in Turkey and Surrounding Area. Geological Society, London, Special Publications 173, pp. 1–23.
Stampfli, G.M., Von Raumer, J.F., Borel, G.D., 2002. Paleozoic evolution of pre-Variscan terranes: from Gondwana to the Variscan collision. In: Martínez Catalán, J.R., Hatcher, R.D.J.R., Arenas, R., Díaz García, F. (Eds.), Variscan-Appalachian Dynamics: The Building of the Late Paleozoic Basement. Geological Society of America Special Paper 364, pp. 263–280.
Streckeisen, A., 1976. To each plutonic rock its proper name. Earth Sci. Rev. 12, 1–33.
Şengör, A.M.C., 1984. The Cimmeride Orogenic System and the Tectonics of Eurasia. Geological Society of America Special Paper, 195 pp.
Sun, S.-S., McDonough, W., 1989. Chemical and isotopic systematics of oceanic basalts: implications for mantle composition and processes. Geol. Soc. Lond. Spec. Publ. 42 (1), 313–345.
Thiéblemont, D., Tegyey, M., 1994. Une discrimination géochimique des roches différenciées témoin de la diversité d'origine et de situation tectonique des magmas calco-alcalins. CR l'Acad. Sci. Paris 319 (II), 87–94.
Thompson, R.N., Morrison, M.A., Hendry, G.L., Parry, S.J., 1984. An assessment of the relative roles of a crust and mantle in magma genesis: an elemental approach. Philos. Trans. R. Soc. Lond. A 310, 549–590.
Torsvik, H.T., Cocks, L.R.M., 2013. Gondwana from top to base in space and time. Gondwana Res. 24, 999–1030.
Ustaömer, P.A., Mundil, R., Renne, P.R., 2005. U/Pb and Pb/Pb zircon ages for arc-related intrusions of the Bolu Massif (W Pontides, NW Turkey): evidence for Late Precambrian (Cadomian) age. Terra Nova 17, 215–223.
Ustaömer, P.A., Ustaömer, T., Collins, A.S., Robertson, A.H.F., 2009. Cadomian (Ediacaran–Cambrian) arc magmatism in the Bitlis Massif, SE Turkey: magmatism along the developing northern margin of Gondwana. Tectonophysics 473, 99–112.
Ustaömer, P.A., Ustaömer, T., Gerdes, A., Robertson, A.H.F., Collins, A.S., 2012. Evidence of Precambrian sedimentation/magmatism and Cambrian metamorphism in the Bitlis Massif, SE Turkey utilising whole-rock

geochemistry and U-Pb LA-ICP-MS zircon dating. Gondwana Res. 21, 1001–1018.
Von Raumer, J.F., Stampfli, G.M., Borel, G., Bussy, F., 2002. Organization of pre-Variscan basement areas at the north-Gondwanan margin. Int. J. Earth Sci. 91, 35–52.
von Raumer, J.F., Stampfli, G.M., Ricardo Arenas, R., Martínez, S.S., 2015. Ediacaran to Cambrian oceanic rocks of the Gondwana margin and their tectonic interpretation. Int. J. Earth Sci. (Geol. Rundsch). http://dx.doi.org/10.1007/s00531-015-1142-x.
Winchester, J.A., Pharaoh, T.C., Verniers, J., Ioane, D., Seghedi, A., 2006. Palaeozoic accretion of Gondwana-derived terranes to the East European Caraton. Geol. Soc. Lond. Memoir 32, 323–332.
Windley, B.F., 1992. Proterozoic collisional and accretionary orogens. Develop. Precambr. Geol. 10, 419–446.
Wu, F.-Y., Yang, Y.-H., Xie, L.-W., Yang, J.-H., Xu, P., 2006. Hf isotopic compositions of the standard zircons and baddeleyites used in U-Pb geochronology. Chem. Geol. 234 (2006), 105–126.
Wu, Y.B., Zheng, Y.F., Zhang, S.B., Zhao, Z.F., Wu, F.Y., Liu, X.M., 2007. Zircon U-Pb ages and Hf isotope compositions of migmatite from the North Dabie terrane in China: constraints on partial melting. J. Metamorph. Geol. 25, 991–1009.
Yazgan, E., 1983. A geotraverse between the Arabian platform and the Munzur nappes. In: Int. Symp. On the Geology of the Taurus Belt. Field Guide Book, Excursion, Ankara.
Yazgan, E., 1984. Geodynamic evolution of the eastern Taurus region. In: Tekeli, O., Göncüoğlu, C. (Eds.), Geology of the Taurus Belt, Proceedings of International Tauride Symposium Mineral Research and Exploration. Institute of Turkey Publications, pp. 199–208.
Yazgan, E., Chessex, R., 1991. Geology and tectonic evolution of Southeastern Taurus in the region of Malatya. Turk. Assoc. Petrol. Geol. Bull. 3 (1), 1–42.
Yiğitbaş, E., Yılmaz, Y., 1996. New evidence and solution to the Maden complex controversy of the southeast Anatolian orogenic belt (Turkey). Geol. Rundsch. 85, 250–263.
Yıldırım, E., 2010. Sincik-Çelikhan (Adıyaman) arasıki magmatik kayaçların petrolojisi F.U (Elazig-Turkey), Ph.D. Thesis, 244 pp.
Yılmaz, Y., 1993. New evidence and model on the evolution of the southeast Anatolian orogen. Geol. Soc. Am. Bull. 105, 251–271.
Yılmaz, Y., Yıldırım, M., 1996. Geology and evolution of nappe area (metamorphic massives) at the Southeastern Anatolian Orogenic Belt. TUB_ITAK Tr. J. Earth Sci. 5, 21–38.
Yılmaz, Y., Yiğitbaş, E., 1991. The different ophiolitic metamorphic assemblages of the SE Anatolia and their significance in the geological evolution of the region. In: Proceedings of the 8th Petroleum Congress, pp. 128–140.
Yılmaz, Y., Yiğitbaş, E., Genc, Ş.C., 1993. Ophiolitic and metamorphic assemblages of southeast anatolia and their significance in the geological evolution of the orogenic belt. Tectonics 12, 1280–1297.
Yılmaz-Şahin, S.Y., Aysal, N., Güngör, Y., Peytcheva, I., Neubauer, F., 2014. Geochemistry and U-Pb zircon geochronology of metagranites in Istranca (Strandja) Zone, NW Pontides, Turkey: implications for the geodynamic evolution of Cadomian orogeny. Gondwana Res. 26, 755–771.
Zheng, J.P., Griffin, W.L., O'Reilly, S.Y., Lu, F., Wang, C., Zhang, M., Wang, F., Li, H., 2004. 3.6 Ga lower crust in central China: new evidence on the assembly of North China Craton. Geology 32, 229–232.
Zheng, J.P., Griffin, W.L., O'Reilly, S.Y., Zhang, M., Pearson, N.J., Pan, Y.M., 2006. Widespread Archean basement beneath the Yangtze craton. Geology 34, 417–420.
Zlatkin, O., Avigad, D., Gerdes, A., 2013. Evolution and provenance of Neoproterozoic basement and Lower Paleozoic siliciclastic cover of the Menderes Massif (western Taurides): coupled U-Pb–Hf zircon isotope geochemistry. Gondwana Res. 23 (2), 682–700.